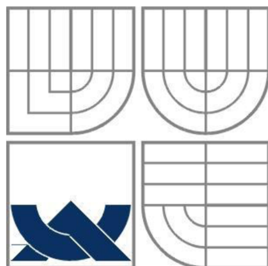

VYSOKÉ UČENÍ TECHNICKÉ V BRNĚ

BRNO UNIVERSITY OF TECHNOLOGY

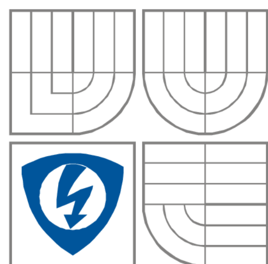

FAKULTA ELEKTROTECHNIKY A KOMUNIKAČNÍCH TECHNOLOGIÍ

ÚSTAV AUTOMATIZACE A MĚŘICÍ TECHNIKY

FACULTY OF ELECTRICAL ENGINEERING AND COMMUNICATION

DEPARTMENT OF CONTROL AND INSTRUMENTATION

TESTOVÁNÍ MEMS GYROSKOPŮ

TESTING OF MEMS GYROSCOPES

DIPLOMOVÁ PRÁCE

MASTER'S THESIS

AUTOR PRÁCE — Bc. Stanislav Hasík

AUTHOR

VEDOUCÍ PRÁCE — Ing. Stanislav Klusáček, Ph.D.

SUPERVISOR

BRNO 2016

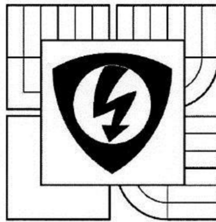

VYSOKÉ UČENÍ TECHNICKÉ V BRNĚ

Fakulta elektrotechniky a komunikačních technologií

Ústav automatizace a měřicí techniky

Diplomová práce

magisterský navazující studijní obor

Kybernetika, automatizace a měření

Student: Bc. Stanislav Hasík | ***ID:*** 146003

Ročník: 2 | ***Akademický rok:*** 2015/16

NÁZEV TÉMATU:

Testování MEMS gyroskopů

POKYNY PRO VYPRACOVÁNÍ:

Cílem diplomové práce je vytvoření měřicího řetězce pro testování MEMS struktur pomocí zařízení Polytec Micro System Analyzer – 500.

1. Zpracujte rešerši týkající klíčových parametrů MEMS struktur určených pro měření úhlové rychlosti.
2. Navrhněte měřicí řetězec pro měření MEMS struktur pomocí zařízení dostupných ve firmě Honeywell International s.r.o. v Brně.
3. Navrhněte způsob automatického ovládání polohovacích zařízení a Peltierových článků umístěných ve vakuové komoře s využitím LabVIEW.
4. Ověřte navržený měřicí řetězec pro měření parametrů na MEMS strukturách – resonator, in-plane gyroskop a to zejména funkčnost navrženého zařízení pro automatické polohování a funkčnost řízení teploty přípravku měřeného MEMS elementu ve vakuové komoře.
5. Proměřte šumovou charakteristiku v závislosti na úrovni vakua u out-of-plane MEMS gyroskopu navrženého a vyrobeného firmou Honeywell International s.r.o.

Diplomovou práci vypracujte v anglickém jazyce. Jednotlivé postupy konzultujte. Práce bude realizována ve spolupráci s firmou Honeywell International s.r.o., divizí Advanced Technology.

DOPORUČENÁ LITERATURA:

1: HUSÁK, M.: Mikrosenzory a mikroaktuátory. Academia, Praha, 2008

2: Volker Kempe, Inertial MEMS - Principles and Practice, March 2011, ISBN: 9780521766586.

Termín zadání: 8. 2. 2016 | ***Termín odevzdání:*** 16. 5. 2016

Vedoucí práce: Ing. Stanislav Klusáček, Ph.D.

Konzultanti diplomové práce: Ing. Tomáš Neužil, Ph.D., Honeywell International s.r.o., AT

doc. Ing. Václav Jirsík, CSc.

předseda oborové rady

UPOZORNĚNÍ:

Autor diplomové práce nesmí při vytváření diplomové práce porušit autorská práva třetích osob, zejména nesmí zasahovat nedovoleným způsobem do cizích autorských práv osobnostních a musí si být plně vědom následků porušení ustanovení § 11 a následujících autorského zákona č. 121/2000 Sb., včetně možných trestněprávních důsledků vyplývajících z ustanovení části druhé, hlavy VI. díl 4 Trestního zákoníku č. 40/2009 Sb.

Abstrakt

Tato diplomová práce se zabývá teoretickými poznatky o konstrukcích a parametrech MEMS gyroskopů. Dále je prezentován navržený měřicí řetězec pro testování MEMS gyroskopů ve společnosti Honeywell International s.r.o. a to zejména s použitím systémů: Polytec MSA-500, goniometrických plošin a kontroléru od firmy Standa a kontroléru pro řízení Peltierových článků. Praktická část diplomové práce obsahuje popis navrženého kontroléru pro řízení teploty testovaného zařízení a také popis aplikace v prostředí LabVIEW („Measurement systém“), která se používá pro řízení pozice dvou goniometrických plošin a pro řízení Peltierových článků. Tento systém je schopen plně řídit pozici goniometrických plošin, zarovnat povrch testovaného zařízení do ideálně kolmé pozice vůči optické hlavě analyzátoru Polytec MSA-500 a také kontrolovat teplotu testovaného zařízení. Závěrečná část diplomové práce je věnována testům základních parametrů MEMS gyroskopů se zaměřením na závislost tzv. Angle Random Walk a offsetu MEMS gyroskopu na kvalitě vakua v prostředí struktury.

Klíčová slova

MEMS Gyroskop, Goniometr, Polytec MSA-500, Peltierův článek, Regulátor.

Abstract

This diploma thesis presents theoretical information regarding MEMS gyroscopes their parameters and designs. The description of measurement chain be used for testing of MEMS gyroscopes in Honeywell International s.r.o. is presented. Special focus is devoted to: the Polytec MSA-500 system, the Standa goniometers and their controller, Peltier cell and its driver. The practical part of this thesis contains the description of the thermal control system and also the description of the developed “Measurement system” in the LabVIEW software which is used for controlling the goniometers position and the Peltier cell. The system is able to fully control two goniometer stages, align the surface of tested MEMS device to orthogonal position with respect to the Polytec MSA-500 measurement head and also control the temperature of the tested device. The last part of this thesis presents the tests of the MEMS gyroscope parameters with special focus to the MEMS gyroscope angle random walk and the bias dependence on the vacuum quality of the structure environment.

Keywords

MEMS, Gyroscope, Goniometer, Polytec MSA-500, Peltier cell, Controller.

Bibliografická citace

HASÍK, S. *Testování MEMS gyroskopů*. Brno: Vysoké učení technické v Brně, Fakulta elektrotechniky a komunikačních technologií, 2016. 63s. Vedoucí diplomové práce byl Ing. Stanislav Klusáček, Ph.D.

Prohlášení

„Prohlašuji, že svou diplomovou práci na téma testování MEMS gyroskopů jsem vypracoval samostatně pod vedením vedoucího diplomové práce a s použitím odborné literatury a dalších informačních zdrojů, které jsou všechny citovány v práci a uvedeny v seznamu literatury na konci práce.

Jako autor uvedené diplomové práce dále prohlašuji, že v souvislosti s vytvořením této diplomové práce jsem neporušil autorská práva třetích osob, zejména jsem nezasáhl nedovoleným způsobem do cizích autorských práv osobnostních a jsem si plně vědom následků porušení ustanovení § 11 a následujících autorského zákona č. 121/2000 Sb., včetně možných trestněprávních důsledků vyplývajících z ustanovení části druhé, hlavy VI. díl 4 Trestního zákoníku č. 40/2009 Sb.

V Brně dne: **16. května 2016** …………………………

podpis autora

Poděkování

Děkuji vedoucímu diplomové práce Ing. Stanislavu Klusáčkovi, Ph.D. za účinnou metodickou, pedagogickou a odbornou pomoc a další cenné rady při zpracování mé diplomové práce.

Děkuji konzultantu diplomové práce Ing. Tomáši Neužilovi, Ph.D. za účinnou metodickou a odbornou pomoc a další cenné rady při zpracování mé diplomové práce.

Děkuji společnosti Honeywell International s.r.o. divizi Aerospace Advanced Technology Europe za umožnění využívat laboratoř inerciálních senzorů a spolupráci při zpracování mé diplomové práce.

V Brně dne: **16. května 2016** …………………………

podpis autora

Contents

1 Introduction 9
1.1 MEMS technology 9
1.2 Gyroscopes 10
1.3 MEMS vibratory gyroscopes 11
1.4 Sensing and driving elements in MEMS technology 12
2 Key parameters of the MEMS gyroscopes 13
2.1 Mechanical performance of vibratory gyroscopes 13
2.1.1 Quality factor (Q-factor) 13
2.1.2 Resonance frequency of MEMS resonator 14
2.1.3 Vibration mode-misalignment error 14
2.2 Electrical performance of vibratory gyroscope 14
2.2.1 Scale factor 14
2.2.2 Zero-rate output (ZRO) 15
2.2.3 Measurement range (input rate limits) 15
2.2.4 Resolution 15
2.2.5 Bandwidth 15
2.2.6 Other parameters 16
2.3 Basics of Allan Variance noise analysis 16
3 MEMS structures for angular measurement 17
3.1 Single mass gyroscope 17
3.1.1 Frame structure for decoupling modes 17
3.1.2 Doubly decoupled frame-free topology 18
3.2 Double mass gyroscope (tuning fork) 18
3.3 Quartz tuning fork gyroscope 19
3.4 Vibrating ring gyroscope 20
3.5 Bulk acoustic-wave gyroscope 20
3.6 Torsional vibratory gyroscopes 21
4 Polytec Micro System Analyzer (MSA-500) 22
4.1 Polytec Scanning Vibrometer (PSV) 23
4.2 Planar Motion Analysis (PMA) 23
4.3 Topography Measurement System (TMS) 24
5 Motorized goniometer stages 25
5.1 Standa motorized goniometer 8MG99V 25
5.2 Standa two-axis controller 26
5.3 The goniometer setup utilization 27
6 Thermal control 28

6.1 The Peltier cell 28
6.2 The driver for Peltier cell 28
6.3 Thermal control setup 30
6.4 The software structure of the thermal controller 31
6.4.1 The identification of the controlled system 33
6.4.2 The PID constants evaluation by Z-N method 34
7 The Measurement System 35
7.1 LabVIEW controller for the goniometer stages 35
7.1.1 The goniometer movement commands 36
7.1.2 The Advanced settings tab of the application 39
7.2 LabVIEW application for the topography measurement 40
7.2.1 The tested gyroscope sample 40
7.2.2 The Polytec MSA-500 topography measurement 41
7.2.3 The topography map in the LabVIEW application 42
7.2.4 The perpendicular aligned surface of the tested device 44
7.2.5 The cursor selection feature of the topography tab 45
7.3 The LabVIEW thermo control system 46
7.3.1 The Thermo controller tab 46
7.3.2 The thermo controller application code 48
7.3.3 The thermo data logger tab 50
7.3.4 The thermo control system performance 51
8 The gyroscope noise analysis 54
8.1 The gyroscope noise over quality of the vacuum 54
9 Conclusion 57
9.1 The summary 57
9.2 The performance 58
References 61
List of attachments 63

1 INTRODUCTION

Today MEMS inertial sensors (gyroscopes, accelerometers, etc.) are widely used in most of the electronic devices of daily use like mobile phones, tablets, GPS navigation and etc. In the sector of consumer electronics the high precision and reliability of the sensors are not the key performance parameters to be sought as the willingness to pay for these high cost features is low in this customer sector. Furthermore, the inertial sensors are used mainly like complementary to other systems and they provide mainly the short term information.

On the other hand MEMS inertial sensors used in the aerospace applications such as navigation systems call for high performance and reliable sensors. In other to test the key parameters influencing accuracy and reliability of whole navigation system there is a need to design and develop special measurement systems and methods to test the sensors already at the beginning of the design process. Main focus is to be given to long term stability and impact of environment – namely temperature in vicinity of the sensor.

The topic of this thesis is dealing with design and development of the complex test system for analysis of the parameters of MEMS gyroscopes intended for Aerospace applications whose development is taking place in Advanced Technology Europe of Honeywell International s.r.o. This chapter provides introduction to the working principles of gyroscopes and MEMS technology.

Other chapters present deeper context of MEMS structures for angular rate measurement. The key parameters of MEMS gyroscopes are defined and basic designs of MEMS gyroscopes are discussed in the detail. Following chapters are dedicated to realization of the measurement system for MEMS gyroscope testing containing thermal stabilization using Peltier cell, as well as stabilization of the MEMS structure with respect to the optical head of the Polytec Micro System Analyzer using goniometers and topography measurement system. The last chapter is devoted to the noise analysis over vacuum quality of Honeywell designed MEMS gyroscope.

1.1 MEMS TECHNOLOGY

This chapter contains short outline to MEMS technology. The specific structures for MEMS gyroscopes are placed in a separate chapter.

MEMS - Micro-Electro-Mechanical Systems is a technology which in simplified way can be described as a miniaturization of mechanical or electro-mechanical structures that are made on silicon based material [1]. The typical size of whole MEMS structure is in order of millimeters and dimensions of single element of microstructure can be under one micrometer.

Technology of the MEMS structures manufacturing is called micromachining or microfabrication. There are many specific techniques of micromachining and it can be divided to two basic categories. The first is bulk micromachining which consists in removing of material by various types of etching (typical case is DRIE - Deep Reactive Ion Etching). The second is surface micromachining which consists in creating extremely small movable structures on surface of the silicon material. Another type of micromachining can be based on lithography which combines both of these types of micromachining.

One of the very frequently used microstructure is called comb (or comb fingers) structure, shown in figure 1 which is typically used like actuator as well as sensing element.

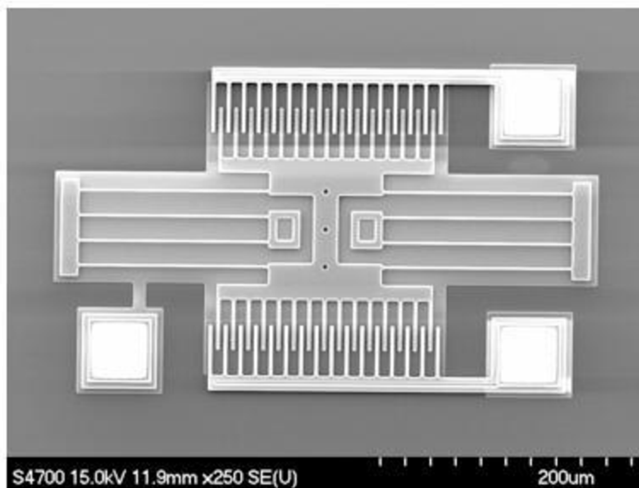

Figure 1: MEMS resonator with comb fingers structure [1]

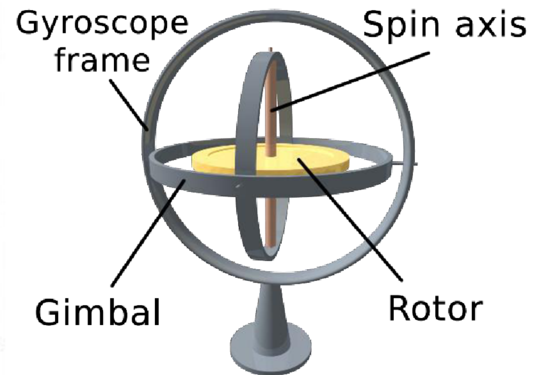

Figure 2: Gyroscope of classic construction [2]

When the voltage is applied to the comb structure there is induced electrostatic force which causes attracting the movable comb structure. This principle is used as a micro actuator. When the movable structure movement is driven by other (external) force it can be used to detect this movement and thus also the external force by change in capacity between stationary and movable comb structures. The typical size of one comb finger is about several microns only, and the numbers of combs can be up to hundreds to increase the force of actuator or to improve the sensitivity of sensing element.

1.2 Gyroscopes

The gyroscope is an inertial sensor for sensing the angular rate and it is simply usable for any angular measurement. Inertial sensors are containing a reference system to compare the measured values independently on the surrounding environment (Earth). The gyroscope is outputting information about orientation in the area independently of its position. It can be used for navigation in universe or anywhere on the Earth as well as in air.

The MEMS gyroscopes principle is typically based on Coriolis force which acts on the moving proof mass. The movement of proof mass can be rotary or linear. Coriolis force is expressed by following equation:

$$\boldsymbol{F} = -2m\overline{\boldsymbol{\Omega}} \times \overline{\boldsymbol{v}} \qquad \text{(eq. 1.1)}$$

F is Coriolis force acting on the proof mass [N]
m is weight of proof mass [kg]
$\overline{\Omega}$ is a vector of angular velocity (rotation of whole system) [rad/s]
$\overline{v}$ is a vector of proof mass velocity (rotary or linear) [m/s]

Implementation of this principle in MEMS technology is relying on the vibrations of the proof mass with velocity $\overline{v}$ producing Coriolis force if the rotation is applied. (1.1).

1.3 MEMS VIBRATORY GYROSCOPES

In case the reference system of the gyroscope is formed by the vibrating plane instead of rotating disc the response to Coriolis force will stay the same. That type of gyroscope has IEE standardized name Coriolis Vibratory Gyroscope.

Vibratory gyroscope is simpler for construction than the classical gyroscope as the proof mass is fixed by springs or flexible beams allowing straightforward implementation in MEMS technology. The Coriolis force causes the vibrating plane is deflected to vibrate in perpendicular direction to the direction of the drive vibrations which is detected by sensing electrodes. There are multiple different implementations of vibratory gyroscopes in MEMS technology outlined in the next chapter.

For better understanding the MEMS vibratory gyroscopes can be split to two basic groups by mode of proof mass vibrations as follows:

- *In-plane vibratory gyroscope:* MEMS gyroscope is one or several movable silicon flat proof masses called planes (see the first part of the figure 3). When the proof mass is driven to vibrations (drive mode) in X axis (in-plane vibrations) and the system is rotated in the direction of Z axis, the Coriolis force causes in-plane vibrations in Y axis called sense mode. As both drive and sense modes are in one plane the gyroscope is called In-plane gyroscope.
- *Out-of-plane vibratory gyroscope:* is depicted in the same model in figure 3 however the axes are swapped as follows: drive mode is in X direction, the gyroscope is rotated by Y axis instead of Z. Coriolis force causes vibrations in Z axis which is pointing out-of-plane which suggest the name of the principle to out-of-plane.

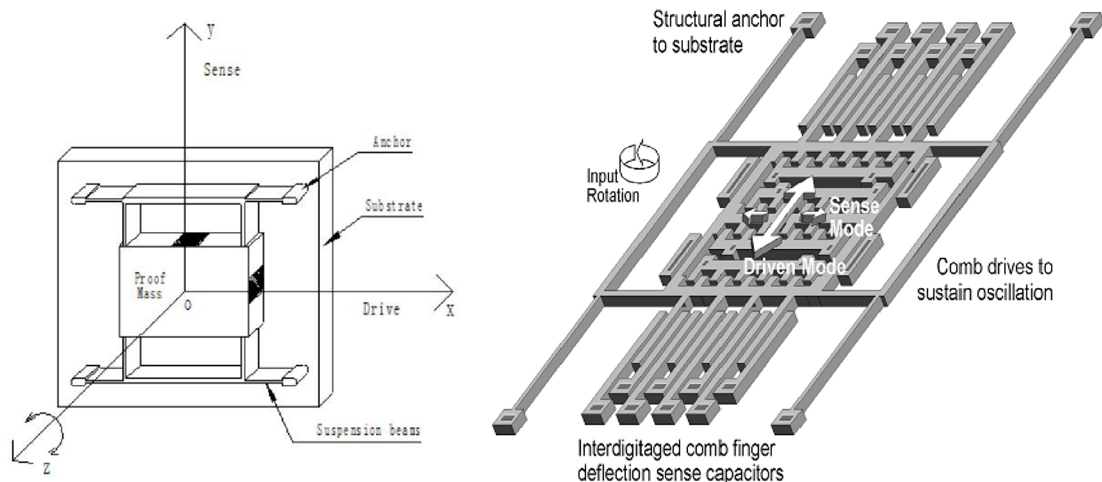

Figure 3: a) In-plane gyroscope model [3]; b) and example of implementation.

The figure 3 b) depicts an example of a simple visualization of MEMS in-plane gyroscope. The inner comb fingers are driven by electrostatic force and vibrate with inner frame of the gyroscope. When the gyroscope is rotated in shown direction the vibrations of the outer frame is produced. These vibrations are detected by the sense comb fingers as change of the capacity between movable and stable comb fingers (difference capacity layout). Because the amplitude of vibrations in sense mode is in order of amplitude smaller than the vibrations in drive mode, the changing of capacity in sense mode is very small thus the fingers are usually much larger than drive mode comb fingers.

1.4 SENSING AND DRIVING ELEMENTS IN MEMS TECHNOLOGY

Short introduction to the basic physical principles of sensing and actuating vibrations of MEMS structures.

- *Electrostatic force:* For actuating of the structures electrostatic force is usually used. This force which acts on the surface of capacitor electrodes results from applying the voltage to the electrodes. This force is proportional to the voltage and the overlap area of electrodes. Electrostatic force is independent on the voltage polarity and it is always attracting force.

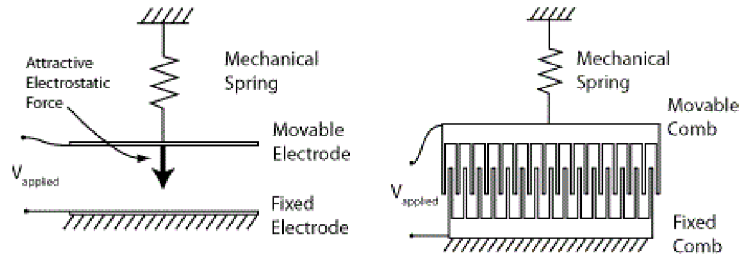

Figure 4: Electrostatic force actuating principle

- *Capacitive displacement sensing:* is contactless method of sensing position of structures which is very straightforward to implement in MEMS technology. The changes in capacity can result from changing the overlap area of the electrode surfaces or by changing the distance between the electrodes. The capacity change of overlapped surfaces can be implemented as two interdigitated comb finger structures (i.e. the drive structure in figure 4 can also be used like sense structure). This principle is, for its small resolution and accuracy, used for sensing of large displacements.

$$\boldsymbol{C = \varepsilon_0 \varepsilon_r \frac{S}{d}} \qquad \text{(eq. 1.2)}$$

C	is capacity [F]
ε_0	is permittivity of the vacuum [F/m] (8.854.10^{-12} F/m)
ε_r	is relative permittivity of the material between the electrodes [-]
S	is the overlapped surface of the electrodes [m^2]
d	is the distance between the electrodes [m]

The capacity change by distance between electrodes provides higher accuracy and can detect small changes of distance however it is a nonlinear function of the measured distance. This nonlinear function can be suppressed by differential connection of sensing electrodes. In the figure 5 the sensing element is connected to form differential capacity combs fingers. When the movable electrode move to one direction that increase capacity of two approaching electrodes and reduce capacity of two receding electrodes. Both dependencies are nonlinear but inverse and serial connection of these capacitors results the linearized function of capacity on the distance. This principle is, however applicable only to small displacement changes.

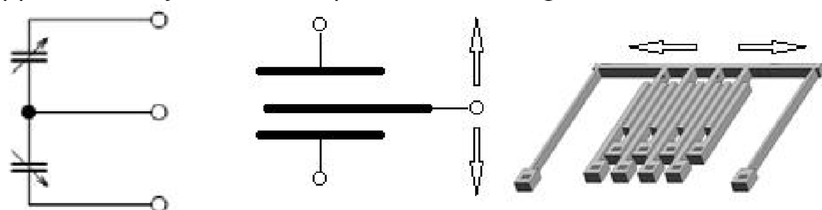

Figure 5: Difference capacity sensing principle

2 KEY PARAMETERS OF THE MEMS GYROSCOPES

The most important parameters can be defined by two different aspects. The first view is from the mechanical performance which is important for development and testing of the gyroscopes. The second view is coming from the electrical performance which describes the accuracy and reliability of tested gyroscope and is widely used for comparison of gyroscopes from different manufacturers.

2.1 MECHANICAL PERFORMANCE OF VIBRATORY GYROSCOPES

All of the mechanical parameters have fundamental influence to many of the electrical parameters, however these parameters are not used directly for comparison of the gyroscopes and typically are considered as internal knowhow of the company.

2.1.1 Quality factor (Q-factor)

Mechanically the MEMS vibratory gyroscope is a simple resonator which filters the input frequencies by its own resonance frequency. If it would be an ideal mechanical oscillator the white thermal noise causes the amplitude of oscillation would grow unlimitedly with every period of oscillation. As the MEMS oscillator is not an ideal one it is losing energy during oscillations due to the damping forces. The magnitude is typically described by Q-factor. The quality factor is dependent on multiple parameters that can be divided to two basic categories by the source of the energy losses. The basic equation defining the quality factor is described in: [4].

$$\boldsymbol{Q = 2\pi \frac{U_{tot}}{U_{diss}} = 2\pi \frac{U_{tot}}{U_{int} + U_{surr}} = \frac{1}{\frac{1}{Q_{int}} + \frac{1}{Q_{sur}}}} \qquad \text{eq. (2.1)}$$

Q Resulting quality factor of MEMS element (resonator).
U_{tot} Total energy of oscillating system at resonance frequency.
U_{diss} Average energy loss during one period at resonance frequency.
U_{int} Intrinsic energy losses (structural based).
U_{surr} Losses by interaction of structure surface and surrounding environment.

The evaluation of values and sources of these losses is very tricky because there is huge amount of parameters and phenomena which influencing them. Basically these are:

- *Intrinsic losses:* If the flexible beam (or spring) is stressed there is an arising surface and volume phenomenon which causing energy losses (heat losses) in the beams. The volumetric effect is negligible because the MEMS has the surface much larger than the volume of material [4]. Intrinsic losses can be reduced by optimal geometry of flexible beams at gyroscope design.
- *Viscous losses:* When the structure is moving in the surrounding environment (typically air or inert gas) that must flow around the structure and there arising the local differences of pressure. That “damping” attenuates the oscillation. For gyroscopes is the damping very undesirable, and typically is reduced by air exhaustion from the space around structure. The pressure must be as low as possible for proper function of the gyroscope.

The quality factor of MEMS resonator in gyroscope is in the tens to hundreds thousands at extremely low pressures.

2.1.2 Resonance frequency of MEMS resonator

This key parameter is defined by the weight of the proof mass and stiffness of flexible beams which are carrying it. The resonance frequency is driving the design of the readout electronics as it drives the proof mass exactly at the resonance frequency. Because the resonance frequency is temperature dependent there must be implemented a control loop for thermal compensation as well as to stabilize the magnitude of vibrations. This is mostly caused by temperature dependence of stiffness of flexible beams.

Some gyroscopes have different resonance frequency of drive mode and sense mode because these has separated drive and sense combs from proof mass by another flexible beams (springs). That type of gyroscope is illustrated at figure 3 b).

2.1.3 Vibration mode-misalignment error

The manufacturing process imperfections cause the proof mass center of gravity is not located in ideally in center of the suspension. When the suspended proof mass oscillate in drive mode the oscillations are not perfectly parallel to the base substrate, and perpendicularity of drive and sense mode of oscillations is not ideal. The proof mass is slightly wobbling during the oscillations and drive oscillations are transferred to sense mode. The mode-misalignment is one of main sources of gyroscope bias or the zero-rate output which will be explained further.

2.2 ELECTRICAL PERFORMANCE OF VIBRATORY GYROSCOPE

The MEMS gyroscope performance provides the performance of the whole sensor system including mechanical elements and the electronics transferring the mechanical movement to measurable signal. These parameters are widely used for comparison of the MEMS gyroscopes:

2.2.1 Scale factor

Or the sensitivity of gyroscope it is a ratio between a value changes in output to a value changes in input. Scale factor is determined by mechanical sensitivity of the MEMS element and the electrical gain which can reach the order of millions to obtain the optimal voltage of the gyroscope output signal. The sensitivity is typically specified in $mV/°/sec$ and is evaluated as the slope of the least squares straight line fit to input-output signal ratio [5]. The scale factor parameter is characterized by unit and its accuracy or error.

- *Linearity error:* Is the maximal deviation of the output value from the best linear fit straight line of input-output sensitivity ratio. It is usually expressed by percentage of full scale or percentage of output value.
- *Nonlinearity:* Is the systematic deviation of curve which defines input-output sensitivity ratio from best linear fit straight line.
- *Asymmetry error:* Is the difference between the scale factor measured with positive and negative input, and with the same amplitudes. It is usually specified like fraction of the scale factor measured over the input range [5].
- *Scale factor stability:* Declared changes of scale factor during specified time of continuous operation and operating conditions: temperature, power supply, etc.
- *Scale factor temperature sensitivity:* It is expressed by percentage of scale factor value or maximal deviation in percentage of full scale. Mechanical sensitivity of MEMS elements is temperature dependent and can be compensated by electronics.
- *Scale factor acceleration sensitivity:* Because the gyroscopes contains the suspended proof mass there is dependence of scale factor (or scale factor deviation) under influence of acceleration. Usually expressed in $°/\sec\ per\ g$.

2.2.2 *Zero-rate output (ZRO)*

Also called Bias or offset of gyroscope and it is one of most difficult phenomena [4]. It is caused by mechanical bias of the MEMS element and by the bias of sensing electronics. It is expressed by the average value of gyroscope output over the specified time within the specified conditions without input rotation. Typical expressing is in $°/sec$ or $°/hr$. Bias is temperature dependent and nominally set to a minimum at room temperature. Besides this static specification there is the random drift rate which is caused by random time-varying part of bias. Random drift rate is usually specified in terms of the Allan variance components [5]:

- *Angle Random Walk (ARW):* Is average angular error measured by integrating angular rate output signal and is typically expressed in $°/\sqrt{hr}$ or in $°/s\ per\ \sqrt{hr}$. It is caused by the white noise component in the gyro rate output which is integrated and thus the angular error increases with time. The ARW is one of the key performance factors as it defines fundamental limits of angular measurements of the integrated rate gyro output. ARW can be also expressed by Fast Fourier Transform or by Power Spectral Density of angular rate signal divided by time in hours.
- *Bias Instability:* Bias instability is typically expressed as a minimum point of Allan Variance curve in $°/hr$ and it represents the best achievable accuracy for fully modeled sensor and including active bias estimation [6]. The long term data of gyroscope output in stable position is required to measure bias value. The bias is then defined as an average value of the measured data and the bias instability expresses the changes of bias during the time of measurement
- *Rate Random Walk (RRW):* Is phenomenon which occurs at very low-frequencies and can be characterized as a drift rate error which it is increasing with time due to influence of white noise in angular acceleration input. Is usually expressed by end of Allan Variance curve in $°/hr\ \mathrm{per}\ \sqrt{hr}$ [5].

Other bias changes are caused by environmental conditions since the parameters of the electronic components are temperature dependent as well as the parameters of the MEMS element itself. Other influences of environment effects such as drift rate acceleration sensitivity, temperature gradient sensitivity are influencing the gyroscope performance as well.

2.2.3 *Measurement range (input rate limits)*

Range of positive and negative rate input that can be detected by the device without saturation of sensing element or sensing electronics. Typical ranges of MEMS vibratory gyroscopes are:

- Yaw rate gyroscopes: ±(50÷300)°/sec
- Rejecting rate gyroscopes: ±(1000 and more)°/sec

2.2.4 *Resolution*

Resolution of MEMS gyroscope can be described as: minimum value in gyro input (rate input) which is greater than input noise level and produces a valid change in gyro output (angular output). Valid change is usually specified like percentage (usually least 50%) of expected value which is corresponding to nominal scale factor. Practically it describes minimal angular rate which can be detected by gyroscope and is expressed as spectral resolution in $°/\sec\ per\ \sqrt{Hz}$

2.2.5 *Bandwidth*

The frequency range of the angle rate input that can be detected by gyroscope. Nominally set by electronics due to cutoff frequency which represented -3dB point. Typical bandwidth of MEMS gyroscope is 10 ÷ 100 Hz of course there are available gyroscopes with bandwidth over 1000 kHz but these has worse noise performance. Therefore the bandwidth is defined by the gyroscope application (e.g. for satellites lower gyroscope bandwidth than for helicopters gyroscope applications is required).

2.2.6 *Other parameters*

- *Turn-on time:* The time needed to produce specified useful output signal from connection gyroscope electronics to power. The useful signal need not necessarily correspond with full specification of the gyroscope performance. This parameter is typically related to the time which is needed to reach the resonance frequency of MEMS resonator to produce valid Coriolis response.
- *Vibration sensitivity:* Is the ratio of change output gyroscope signal due to influence vibrations in linear or angular directions.
- *Shock resistance:* Maximum shock that the operating or non-operating gyroscope can endure without sensor failure and can continue in operation with defined performance.
- *Standard parameters:* Such as power supply voltage, power supply consumption, packaging and size, storage and operation temperatures and etc.

2.3 BASICS OF ALLAN VARIANCE NOISE ANALYSIS

In a nutshell, Dr. David Allan developed the method of oscillator noise analysis for clock systems to improve the stability and performance of GPS devices as the accuracy depends on stable clock source. The MEMS gyroscope contains the resonator (oscillator) therefore the method can be easily adapted to evaluate the noise and bias performance of the gyroscope as well.

The Allan Variance is the time domain analysis which analyze time sequence of data to pull out intrinsic noise in the system as a function of averaging time [6]. Basically a long term sequence of data is taken and divided into frames with the same time τ. The average value of the data in each frame is computed and the differences between successive frames is determined. After this sum of a squared differences is produced and the result is divided by "rescaling factor" [6] and square root is computed. Now we increase the time of frames τ and start over until about 9 frames to average is achieved. Basic equation can also be found in [6].

$$\boldsymbol{\sigma(\tau)^2 = \frac{1}{2(n-1)} \sum_i (y(\tau)_{i+1} - y(\tau)_i)^2} \qquad \text{eq. (2.2)}$$

τ averaging interval (time of frame)
n number of frames
i actual frame
y average value of input data frame
$\sigma(\tau)$ Allan Variance curve (dependence on averaging interval)

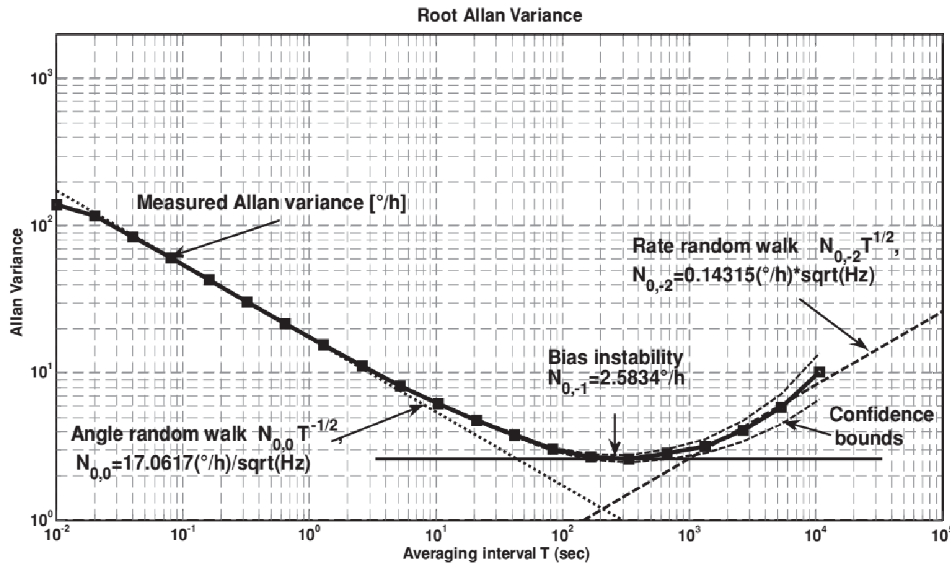

Figure 6: Example of Allan Variance noise analysis [4]

3 MEMS STRUCTURES FOR ANGULAR MEASUREMENT

In following text the basic principles of MEMS elements for angular rate sensing operation are presented and the basic advantages and disadvantages of individual approaches are discussed. The design, implementation or modeling of the MEMS elements is not the topic of this thesis.

3.1 SINGLE MASS GYROSCOPE

This type of gyroscope contains one movable proof mass hanged in the suspension formed by flexible beams. It represents one of the simplest designs of the MEMS gyroscope with in-plane or out-of-plane movable proof mass. The in-plane or out-of-plane operation is dependent on flexible beams design and capacitive sensing design. In the figure 7 the example of the gyroscope with H-type suspension [5] is shown.

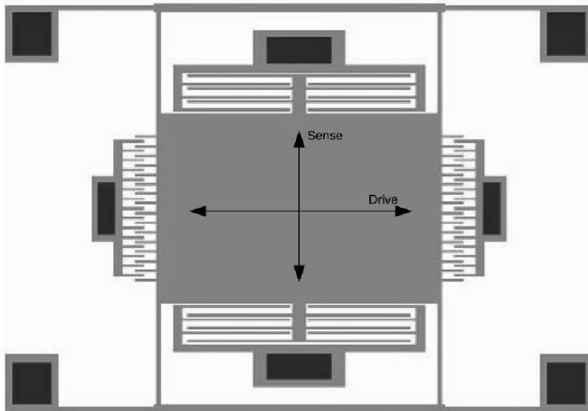

Figure 7: H-type suspended proof mass [5]

The advantage of this gyroscope type is the simplicity of implementation on MEMS structure especially in case of the in-plane movable proof mass.

However the significant disadvantage is very strong coupling between the drive and sense modes of vibrations as the proof mass is movable in 2D directions and the amplitude of drive mode is in the orders of amplitude larger than the one in sense mode. That is visible in figure 7, the drive mode movement can easily induce the movement in sense mode.

3.1.1 Frame structure for decoupling modes

The mode coupling is the significant problem of the single mass gyroscopes. One of the ways how to achieve a better mode decoupling is the use of a frame to separate the drive and sense movements. It can be simply implemented by two types of frames, the first is called drive frame and the second is sense frame.

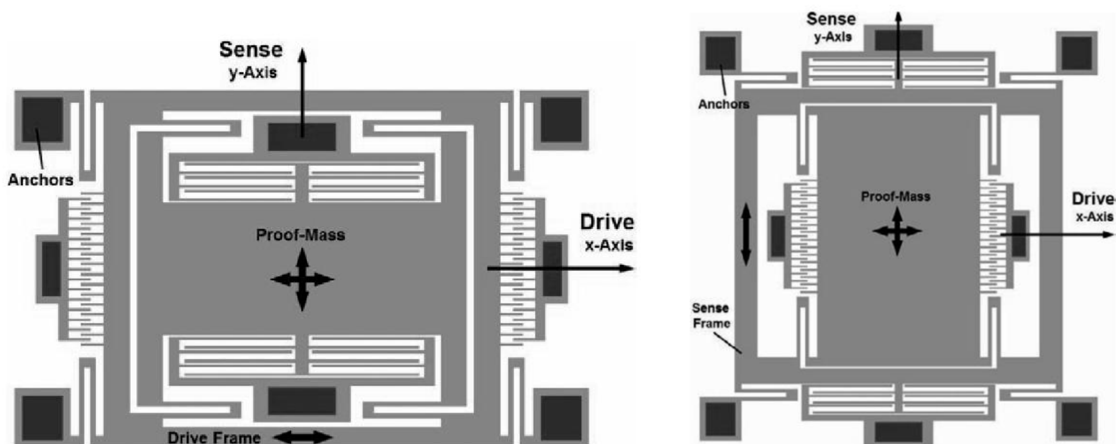

Figure 8: Frame decoupling structures: a) Drive frame, b) Sense frame [5]

The drive frame is stabilizing the drive motion along the drive axis and decreases the drive-to-sense coupling to minimum, however the sense electrodes are still movable in the direction of the drive mode and can induce capacity changes in case of imperfectly parallel surfaces of sensing electrodes. In the opposite case, the sense frame stabilize the sensing electrodes that can move only in the sense direction but the stabilization of the drive movement missing.

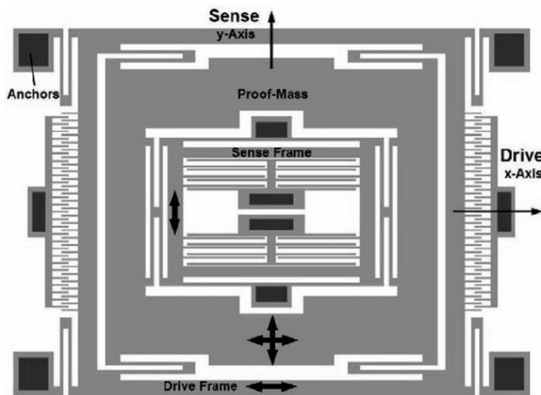

Figure 9: Double frame gyroscope [5]

The best concept is to implement both of these frames nonetheless it also increases the complexity of the design and places increased demands to micromachining processes. Multiple different concepts of double frame gyroscope are implemented in todays off the shelf gyroscopes. An example of one of the simpler concept is based on patented Bosch design (see figure 9) of double frame gyroscope which contains one large drive frame surrounding the proof mass and second small sense frame situated inside of the proof mass. As such the design combines advantages of both frames.

3.1.2 Doubly decoupled frame-free topology

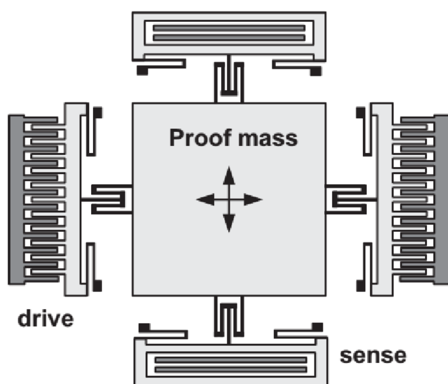

Figure 10: Frame-free gyroscope [4]

Design is similar to double frame design, however the frames fixing the electrodes together are not implemented, rather there are four separate frames (cross beams) which stabilize only one set of electrodes (comb fingers). Each stabilized comb structure can move only in one axis and is prevented against the orthogonal movement. The proof mass is suspended symmetrically between the crossbeam structures by springs. Although this approach is simpler for implementation the achievable performance is not very high.

3.2 DOUBLE MASS GYROSCOPE (TUNING FORK)

Gyroscopes are inherently sensitive to external vibrations and shocks because the proof mass is sensitive to accelerations such as a proof mass in the accelerometers. When the gyroscope is under influence of ambient acceleration or shocks, there is a response in gyroscope output and measurement of small rate amplitudes can be easily disturbed. To obtain high precision gyroscopes one needs to achieve some vibration immunity.

That gyroscopes are called anti-phase also known as tuning fork gyroscopes (TFG) [5]. In TFG there are two identic proof masses implemented which are driven in opposite directions (anti-phase). The Coriolis force caused by the rotation causes the movement of the proof masses in opposite directions. The differential sensing technique to detect proof masses movement can be implemented. The movement of the proof masses in same direction (caused by external acceleration) is thus eliminated. In order to achieve perfectly opposite movement of the proof masses the springs coupling the proof masses are implemented.

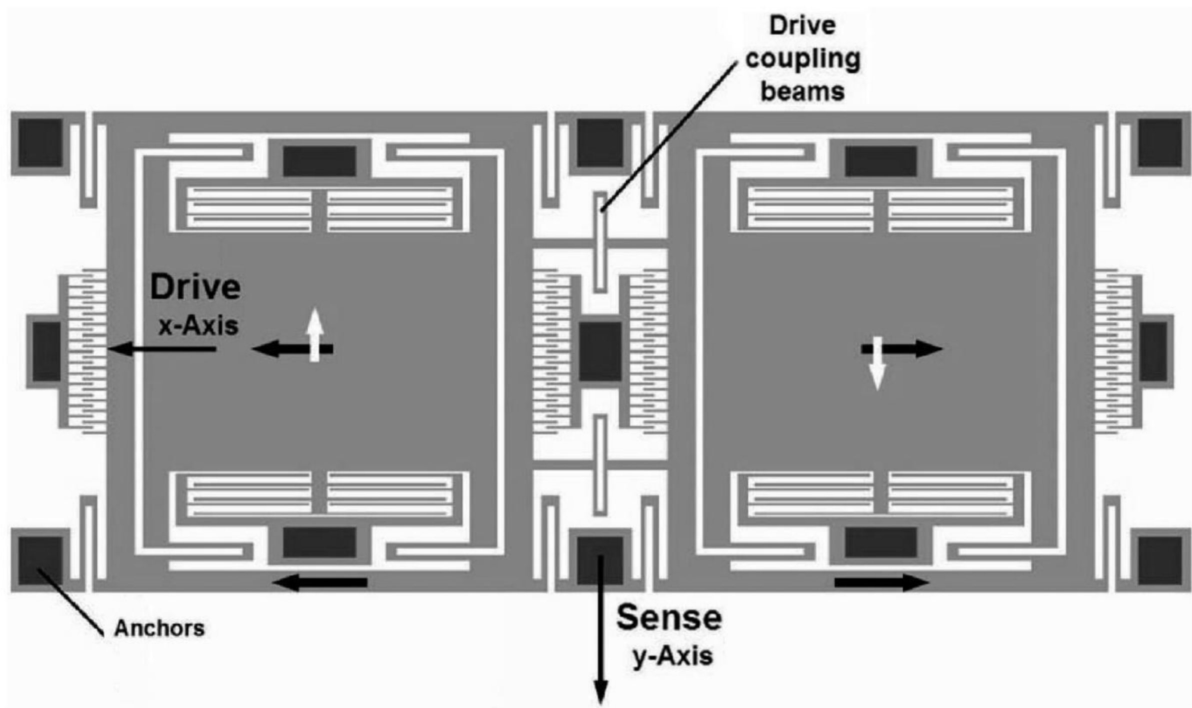

Figure 11: In-plane Tuning Fork Gyroscope [5]

This type of the gyroscope can be implemented both as in-plane and out-of-plane. The implementation depends on flexible beams design which allow (or not allow) out-of-plane proof mass movement and type of sensing elements (combs or parallel planes).

3.3 QUARTZ TUNING FORK GYROSCOPE

One of the older design of vibrating gyroscopes but at its time was one of the best performing gyroscopes. Firstly developed as a metal construction and later as a silicon structure manufactured by MEMS technology. The piezoelectric material for generating and sensing vibrations is used which allows to achieve high-quality drive vibrations and low-noise sensing. These gyroscopes have typically good bias and noise levels, and also good scale factor. For its complicated technology process of production (the length of the fork structure, implementation of piezoelectric material, suspension, etc.) these were replaced by modern (more complex) gyroscope structures.

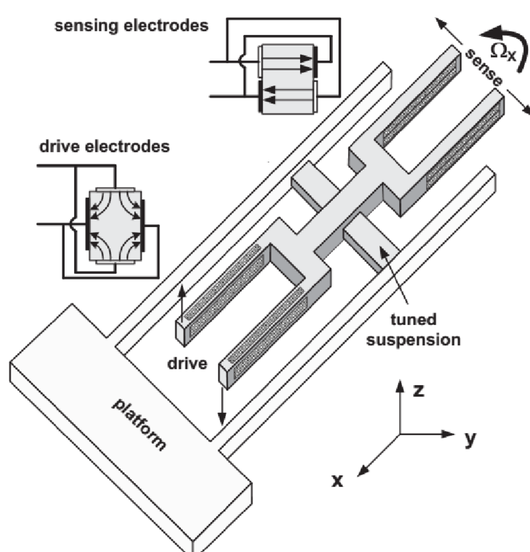

Figure 12: Quartz tuning fork gyroscope [4]

In figure 12 typical implementation of quartz tuning fork gyroscope is depicted. One of the forks is used for drive vibrations (out-of-plane direction). The vibrations are caused by applying voltage to drive electrodes which are made from piezoelectric material (at MEMS technology usually piezo-ceramic). That drive vibrations are decoupled by tuned suspension. In case the structure is rotated there is an in-plane vibration of the sense fork. The sense vibration are sensed by another piezo-ceramic material. The orientation of electrodes is dependent on the direction of the vibrations (in-plane, out-of-plane). In order to achieve good quality resonator and thus acceptable sense performance the electrodes length is to be about 8 mm and more.

3.4 VIBRATING RING GYROSCOPE

One of the simplest implementation of in-plane MEMS vibration gyroscope is shown in figure 13. The gyroscope is formed from one flexible ring attached by flexible springs surrounded by several capacitive electrodes. The ring is driven to the vibrations by the electrostatic force of drive electrodes in one direction. When the structure is rotated the Coriolis force transfers vibrations to another flexural mode of the ring which is shifted by 45° from the drive mode. The sense vibrations are then detected by the other capacitive electrodes as a change of capacity.

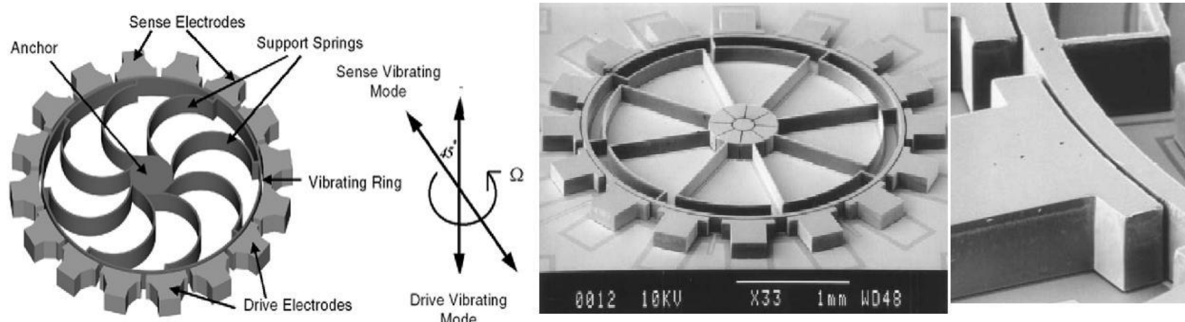

Figure 13: Vibrating ring gyroscope: Principle of operation, example of MEMS implementation on glass substrate by silicon-on-glass technology and detail of capacitive electrode with 8 µm sense gap [7]

In the figure above multiple additional electrodes around the vibrating ring are visible. These electrodes are used for control of the drive vibrations amplitude, and balancing the sense and drive modes in order to minimize the effects of microfabrication process imperfections. The vibrating ring gyroscope is simple and good reliable device with high scale factor, high quality factor of resonator, low output noise and high resolution with temperature compensation. The disadvantage is, however the lower robustness against vibrations and shocks.

3.5 BULK ACOUSTIC-WAVE GYROSCOPE

Structurally similar to vibrating ring gyroscope but bulk silicon disc instead of ring is used. The drive and sense capacitive electrodes are alternating around the disc, and because the acoustic waves (“high-frequency vibrations with small amplitude”) are used there is need to minimize the gap between disc and electrodes for better capacitive sensing resolution.

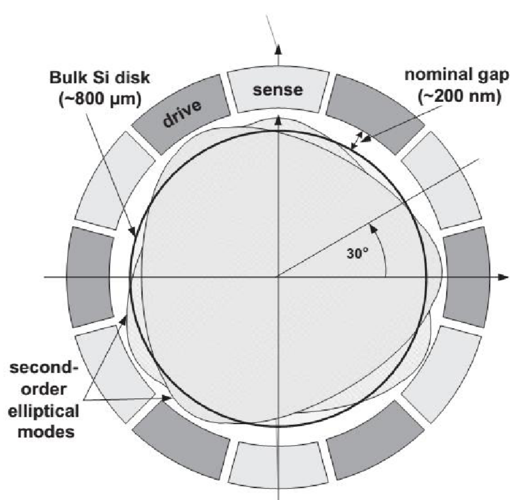

Figure 14: Bulk acoustic-wave gyroscope [4].

Two second-order elliptical acoustic modes to centrally suspended silicon disc are excited by electrostatic drive electrodes. The Coriolis force acting on bulk silicone particles and transfers the energy of vibrations from drive mode to sense mode, and changes the amplitude of sense vibrations. These two modes are shifted by 30° as well as sensing and driving electrodes. These two modes are illustrated in figure 14. Huge advantage of this in-plane gyroscope is in using of resonance frequency in orders of MHz and good low-noise and bias instability result. However the development of this gyroscope is still in progress.

3.6 TORSIONAL VIBRATORY GYROSCOPES

This type of gyroscope (sometime called like rotation-based vibratory gyroscope) is principally similar to single mass translational gyroscopes discussed in chapter 3.1. The main difference is the use of rotational vibratory motion in drive and sense mode.

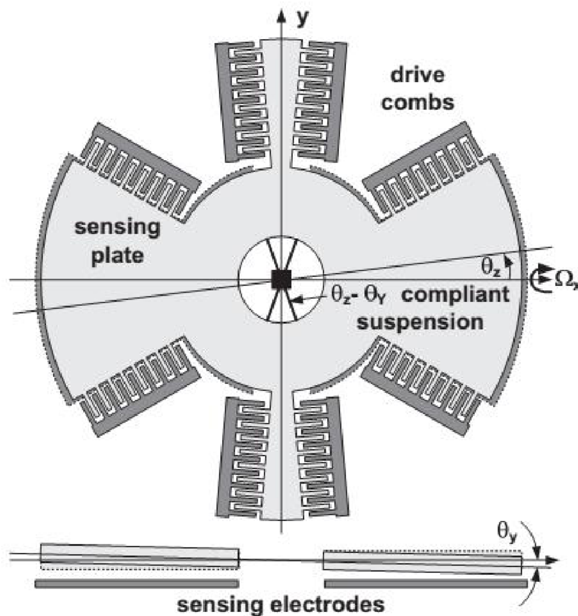

Figure 15: Torsional gyroscope system [4]

The drive mode is in-plane motion around Z-axis illustrated like angular vibrations θ_z excited by drive combs. In case the angular rotation in X-axis is applied the Coriolis force causes out-of-plane rotational vibrations in Y-axis illustrated like θ_y. For sensing vibrations the difference capacitive technique is used. There are implemented two parallel sensing plates around the proof mass. Therefore the sensing capacitance can be very high which provides good scale factor. However, the misalignment error can be quite higher due to central suspension. The other parasitic effects are similar to linear gyroscopes includes the coupling.

The decoupling frames for decoupling sense and drive modes can be used as well as in case of translational vibratory gyroscopes. One of possible implementation is illustrated in figure 16. The drive mode is rotational in Z-axis, however the rotation is decoupled from sensing frame by torsional springs. The sensing frame is stabilized against motion in drive mode however is flexible in the sense mode. The Coriolis force produces out-of-plane rotatory movement of the sensing frame which it is monitored by difference capacitive sensing electrodes.

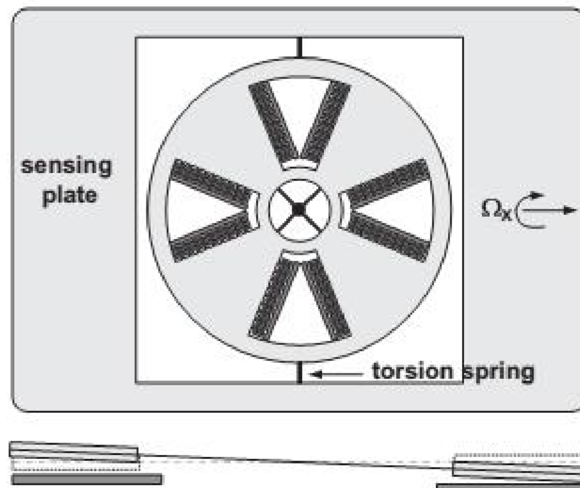

Figure 16: Decoupled torsional gyroscope [4]

These torsional gyroscopes can be implemented like torsional tuning fork design as well as the translational gyroscopes. There are used two torsional systems which are driven in opposite directions and the sense motion is also differential (or anti-phase) for better toughness against to environment vibrations and accelerations. The torsional gyroscopes performance is similar to linear gyroscopes. The main difference is in the technology manufacturing process of the MEMS structures. There are also other implementation of torsional gyroscopes e.g. the system with in-plane sensing and out-of-plane drive or multi-dimensional gyroscopes which are sensitive in more than one axis that are called 2D or 3D gyroscopes.

4 POLYTEC MICRO SYSTEM ANALYZER (MSA-500)

The several chapters above contains the key parameters of gyroscopes and the construction differences between the topologies. This chapter is devoted to the measurement system for testing the intrinsic gyroscope parameters. One of the ways how to measure the gyroscope key parameters is the connection of the MEMS gyroscope to an electronic setup, test the device and evaluate the standard parameters as the scale factor, the zero rate output, the bias instability, etc. However the electronics is another source of measurement uncertainty which is added to the gyroscope output, especially the gyroscope bias therefore the measurements with electronic setup can be degraded typically by the electronic intrinsic noise.

The Polytec MSA-500 is able to measure the gyroscope performance of sense or drive vibrations and the gyroscope mode misalignment directly using the optical beam. However the open structure gyroscope (gyroscope without package) and the vacuum chamber to achieve low-pressure conditions is needed for this type of measurements. The displacement measurement can be performed optically across transparent lid on the vacuum chamber. The Polytec MSA-500 is complex system which combines three individual systems as follows:

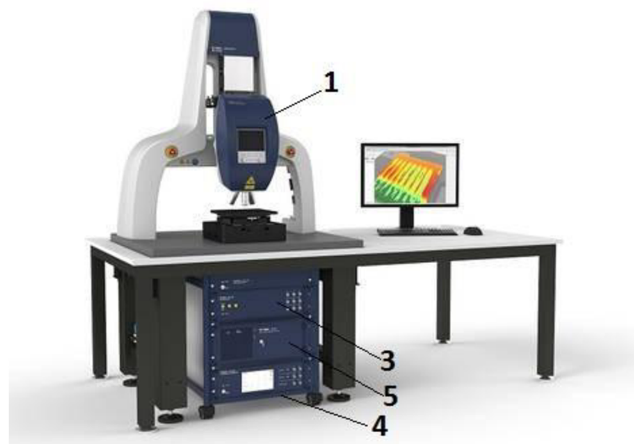

Figure 17: Polytec Micro System Analyzer [8]

Description:

1. The optical unit OFV-552 contains: small monitor for adjustments and focuses the measured object, four changeable microscope lenses on revolving platform, LED illumination unit and progressive scan video camera.
2. The laser unit contains: source of laser beam, beam splitters for divide laser beam to reference and measurement and the laser detector to detect the interferometry of the laser beams. (not visible in the figure 17)
3. The junction box MSA-E-500 is a terminal box for all signals, provides power source for sensors and procures the measurement.
4. The vibrometer Controller OFV-5000 procures the Laser Doppler Vibrometry (LDV) measurement and there is decoded the Doppler velocity to displacement.
5. PC with installed Polytec MSA Software, sets the measurement sequences, makes the post processing and stores the measured data. There is installed the Microsoft operating system and the PC is able to support another measurement software especially the NI LabVIEW.

4.1 POLYTEC SCANNING VIBROMETER (PSV)

The Polytec software for out-of-plane vibration measurement and provides the Scanning Laser-Doppler Vibrometry. The Laser-Doppler Vibrometer (LDV) uses the interferometry principle to detect the Doppler frequency shift caused by velocity of the moving object. However the LDV interferometry principle requires coherent and monochromatic source of light therefore the red Helium-Neon laser source with wavelength $632\ nm$ is needed.

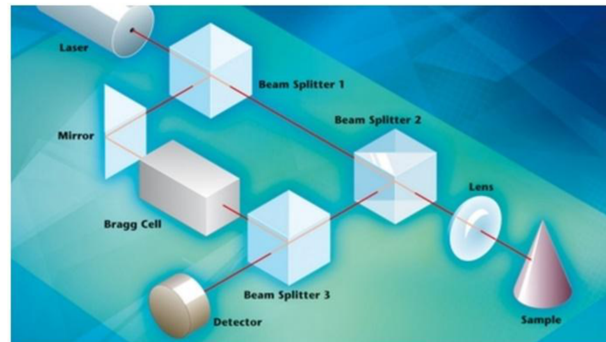

Figure 18: The Laser-Doppler Vibrometer [9]

The LDV principle of operation can be described as follows: the source of laser beam is divided to two separated laser beams as the reference and the measurement beam. The reference beam is focused directly to the laser detector. The measurement beam is focused to the measured object, there is reflected and the movement of the object exactly causes the frequency changes of the laser beam. The reflected beam is optically focused to the detector along the same trajectory as the reference beam. There the beams interfere and the detector detects the frequency shift of these interfering beams as the amplitude changes. To the reference beam trajectory can be placed the Bragg cell unit to achieve the laser beam modulation at high frequencies ($40\ MHz$ [9]) and therefore the system is also able to detect the direction of the velocity. In the MSA-500 system are the reference beam and the measurement beam guided via the optical fibers to the optical unit and there are focused to the measured object. This configuration allows the differential measurements which suppresses the surrounding undesirable vibrations. The measurement head is also able to aim the reference and the measurement beam to the different locations and performs the scanning Laser-Doppler Vibrometry. The resolution of the MSA-500 LDV system is $0.1\ pm$ [8].

4.2 PLANAR MOTION ANALYSIS (PMA)

The Polytec software for in-plane vibrations measurements is provided as the Stroboscopic Video Microscopy. This system uses the green LED illumination unit and the progressive scan video camera for the in-plane vibration measurement however the video camera system is also available for the others measurements which allows visual information about the measured object.

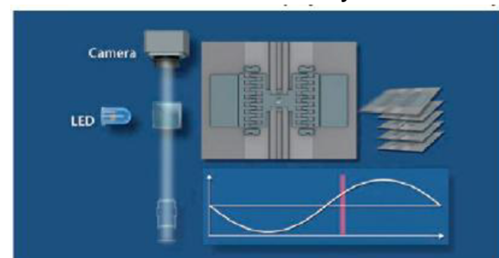

Figure 19: The Stroboscopic Video Microscopy [8]

The PMA is provided by ultra-short (stroboscopic) pulses ($< 80\ ns$) of light and very fast high resolution video capturing (see the figure 19). The system is taking the “shots” or images wherein the in-plane motion looks as static. Due to capturing and reconstructing of these shots is compiled slow motion analysis of the movement. However the frequency of the in-plane movement must be fully synchronized with light pulse generator therefore the system contains the external source of synchronization signal. In case the external synchronization source is unavailable the system also contains the internal generator with frequency sweep and lock functions. The system is able to detect the in-plane vibrations with frequency $1\ MHz$ and resolution $1\ nm$.

4.3 TOPOGRAPHY MEASUREMENT SYSTEM (TMS)

The Polytec software for the surface topography analysis uses the White Light Interferometer. The system uses the green LED illumination unit, progressive scan video camera and special topography objective (Mirau White Light Interferometer objective with z-stage).

The principle of operation is similar to LDV however there is used a LED "white" light source instead of monochromatic source. The White Light Interferometer is based on Michelson interferometer shown in figure 20.2. The source of light beam is divided to the reference and the measurement beam. The reference beam is reflected from the stationary perpendicular mirror (the reference plane). The measurement beam is reflected from the measured object surface and both of the reflected beams are focused to the camera along the same trajectory.

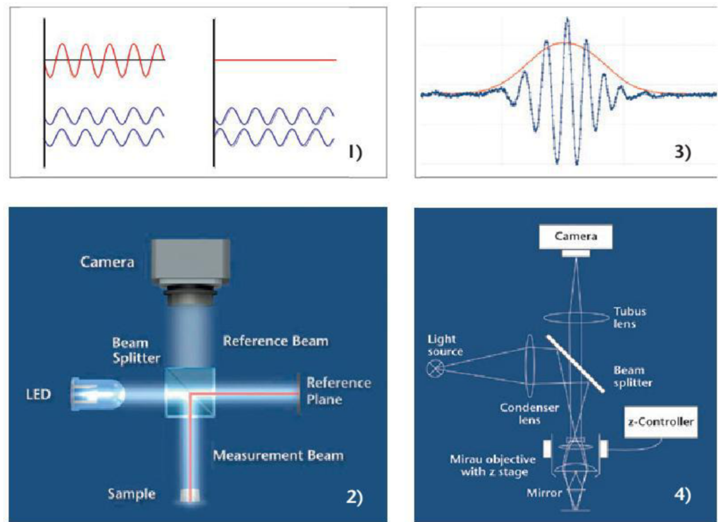

Figure 20: The White Light Interferometry principle [8]

The interference can be destructive or constructive (see the figure 20.1) which dependents on the trajectory length differences of the beams. The camera is detecting interference maxima and minima according to surface topography. In case the light of one wavelength (monochromatic) is used the interference fringes occurs with the multiples of the wavelength. However when the measured surface has a large steps the number of fringes can be missed and the measurement is degraded.

In case the white source of light (polychromatic) is used the constructive interference occurs only in small range of the distances with autocorrelation function form (see the figure 20.3). To achieve the required range of the measured distances the position of the reference mirror must be changeable. This system is illustrated in the figure 20.4, the Mirau objective is changing the position of the installed mirror by the measurement controller and due to is increasing the measurement range. Moreover in this system is the line width narrow enough to give the light source a color, e.g. a green LED [8].

Figure 21: The Nikon Mirau Interferometer lenses

The measurement range depends on the changeable step distances (count and size) of the reference mirror therefore many different lenses is available. The lens used for the following measurements is the Nikon Mirau lens with $10 \times$ zoom, $250\ nm$ range and $87\ nm$ step size. The measurement accuracy depends on the surface structure and it is from hundreds of pm to tens of nm.

5 MOTORIZED GONIOMETER STAGES

The goniometer stage is the system for very precise angular actuating of a movable plate and sometimes it is called a goniometer table. The goniometer is a mechanical equipment which contains one stable plate (surface) attached to the work place and one movable plate where the tested device is mounted. The goniometer motion is not exactly angular however the movement is situated along round trajectory with defined radius. The reference point of the radius is placed to the defined height from the goniometer surface area.

Figure 22: Motorized goniometer stage (example)

To the goniometer movable plate can be installed another goniometer stage to achieve the two-dimensional angular movement of tested device. The goniometer drive can be manual, motorized or both of them. The engine for drive is usually the stepper engine however it can also be the DC engine with absolute speed sensor.

The stepper engine is simple type of electrical engine there is a stator with coils and a rotor made from permanent magnets. The engine rotation is caused due to current direction changes (direction of magnetic field) in steps. Each current direction step causes the angular step of the engine shaft and it is defined by the manufacturers in steps per revolution. The stepper engine can be controlled in the open loop therefore the revolutions are strictly defined by the current steps. However the stepper engine can lose the step in overloaded conditions and then the position of the shaft is unknown. On the other hand the DC engines must be involved in a feedback with the controller. The feedback must be connected to the absolute speed sensor (resolver or optical encoder) therefore the incremental speed sensors are unusable. The goniometer movable plate is generally connected to the engine shaft via high precise Worm Gear Drive (radial gear without play).

5.1 STANDA MOTORIZED GONIOMETER 8MG99V

The goniometers used for the following measurements are two vacuum compatible goniometer stages from the Standa Ltd. Company. The setup allows two axis angular adjustment (two-dimensional) with one center of rotation in $5\ cm$ above the surface. The goniometers are driven by the stepper engines and each has two limit switches. The top surface has seven mounting holes to attach the tested device.

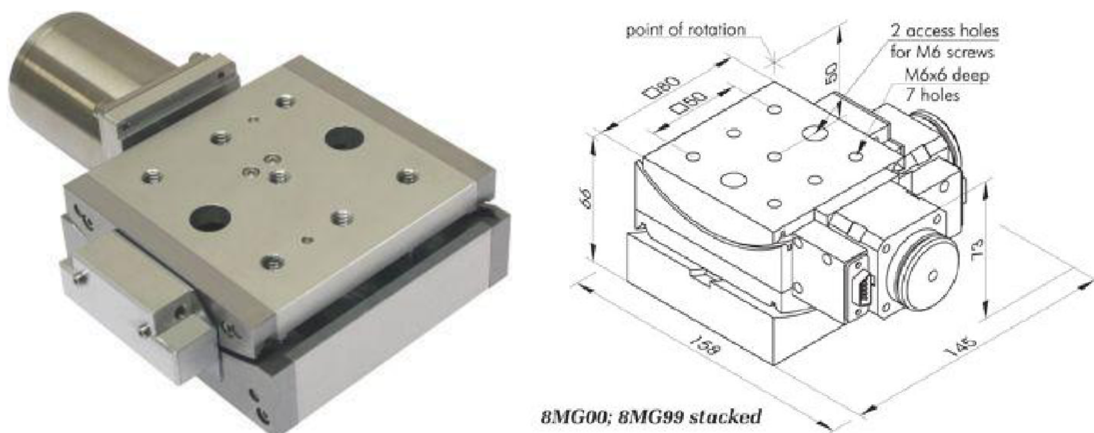

Figure 23: Standa motorized goniometers, 8MG99V – 80 and drawings of setup [10]

The goniometers have slightly different designation and parameters according to its position in the setup (the top one or the bottom one). The specific parameters are shown in table 1.

Table 1: The goniometer parameters

	Position of goniometer	Bottom	Top	
	Designation	8MG99V - 80	8MG99V - 50	
	Travel range	±2.5°	±2.8°	
	Resolution per step	10.96”	16.12”	
	Height of center	80 mm	50 mm	

The other parameters are the same for both of them. The maximal load capacity is $2\ kg$ however the bottom goniometer must carry the weight of the top one which is $1.2\ kg$. Therefore the actual load capacity of the full setup (figure 23) is $0.8\ kg$ for tested device. The goniometers have the bipolar stepper engines (Standa designation 4233). The engine is standard $12\ V$ electrical stepper engine with phase current $0.4\ A$ and with $200\ steps\ per\ revolution\ (1.8°/step)$ – the angular steps of the engine shaft.

The differences of the goniometers allows the construction of the two dimensional setup with one point of rotation in $5\ cm$ above the top surface. When the scanned surface is placed in this height the goniometer angular movement does not cause translational movement of the scanned surface.

5.2 STANDA TWO-AXIS CONTROLLER

The stepper engines requires a power driver. The driver for stepper engines is not difficult to develop however the Standa Ltd. Company offers the compact two-axis controller. The solution is (8SMC4-USB-B9-2) universal motor driver for two stepper engines or two DC engines with speed sensors and importantly the driver is compatible with NI LabVIEW software.

Figure 24: Standa 2-axis controller 8SMC4-USB-B9-2 - Front and back view [10]

The controller communicates with PC via the standard USB 2.0 cable. The goniometers are connected to the controller via two 15-pin d-Sub connectors at the controller back side. The controller is also able to drive the engines manually by the two green buttons at the front panel. For programmatically engine drive there is prepared the library for the LabVIEW environment from Standa Ltd. therefore the controller communicates due to normalized commands with angular position. However the angular normalization is not set automatically and must be set individually for each goniometer. The goniometers have two limit switches which activity is indicated at the front panel. The other features of the controller (linear and rotational encoder connections) are unused.

5.3 THE GONIOMETER SETUP UTILIZATION

The goniometer stages are, inter alia, used for slope compensation of tested device surface to achieve better accuracy of out-of-plane measurement through Laser Doppler Vibrometer. The LDV measures the out-of-plane movement with high accuracy which is useful to examination the mode misalignment of tested gyroscope and it also allows to identify the sources of the gyroscope Zero Rate Output. However, in case the gyroscope proof mass is not ideally perpendicular to the optical head of LDV the drive in-plane vibrations can be optically transferred to the measurement beam according to theoretical assumption [11]:

$$\boldsymbol{v_{LDV}} = \boldsymbol{v_Z} \cdot \boldsymbol{cos(\alpha)} + \boldsymbol{v_X} \cdot \boldsymbol{sin(\alpha)} \qquad \text{eq. (5.1)}$$

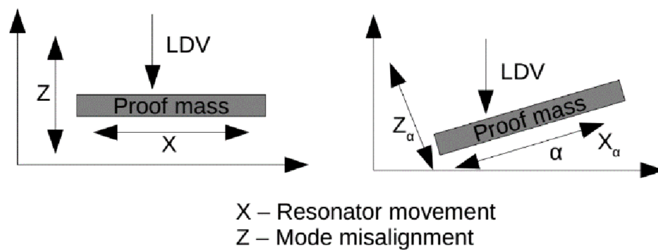

Figure 25: The mode misalignment measurement error

The figure 25 presents the outline of typical measurement setup for direct testing of gyroscope mode misalignment. The gyroscope proof mass is oscillating in in-plane direction the vibrations are transferred to the out-of-plane direction due to mechanical imperfections and causes the Zero Rate Output of gyroscope. Then the mode misalignment is intercepted by the LDV system and its point of origin can be revealed. However in case the in-plane vibrating proof mass is not in ideal perpendicular orientation to the Polytec measurement head the mode misalignment vibration amplitude is decreased by the slope of the proof mass and the in-plane drive movement is directly (optically) added to the measured value of the mode misalignment due to equation 5.1. Moreover the in-plane drive movement is in order of amplitude higher than the out-of-plane misalignment which is increasing the measurement error. The system used, inter alia, for angular slope compensation of the tested gyroscope surface in vacuum chamber is shown in figure 26:

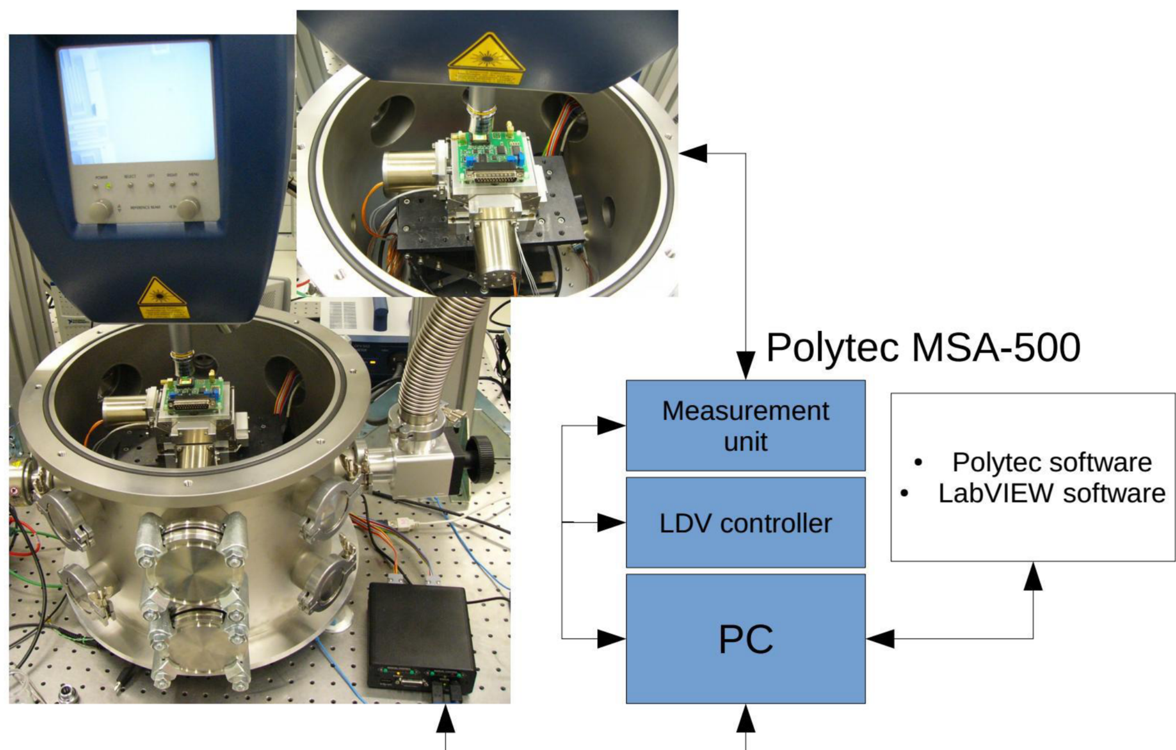

Figure 26: The presentation and the block diagram of the goniometer setup

6 THERMAL CONTROL

For the long term data acquisition in the vacuum chamber must be the tested device temperature stabilized since the device under test heats up during its stress. Therefore the developed measurement chain contains the automatic temperature control of the Peltier cell using the LabVIEW software.

6.1 THE PELTIER CELL

The Peltier cell, also known as: the Peltier module, the Peltier element or the Thermo-electric cooler, is the device based on the Peltier phenomenon which is the opposite phenomenon to the Seebeck phenomenon which was discovered earlier.

The Seebeck phenomenon arises in the junction of two different electron work function materials, in case the temperature difference between the connected and the unconnected ends is applied. Due to the Seebeck phenomenon the voltage potential arises at the unconnected ends. On the other hand due to applying the voltage potential at the unconnected ends the Peltier phenomenon causes the temperature difference between the connected and the unconnected ends.

The thermo-electric cooler is the application of the Peltier phenomenon to achieve a thermal difference between the hot and the cold side of the Peltier cell. In commercial Peltier cells are usually used two semiconductor types (the P-type and the N-type) which are individually formed to small cubes (the P-type cube and the N-type cube) and these cubes are in pairs fitted into a matrix. Then the cubes are serially connected to a chain and arranged to achieve the cold and the hot side of the Peltier cell (see figure 27). When an electrical current is flowing through this structure the Peltier phenomenon causes a thermal difference between the cold and the hot side of the Peltier cell.

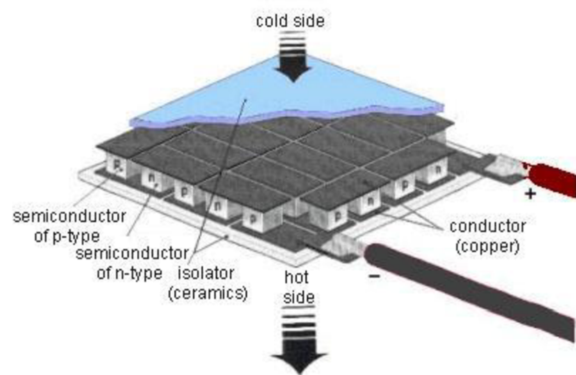

Figure 27: Peltier cell - principle of operation [12]

6.2 THE DRIVER FOR PELTIER CELL

The thermo-electric cooler with the Peltier cell can also be used as the thermo-electric heater this depends on the current orientation passing through the Peltier cell. This feature allows to achieve better temperature stabilization of tested device in vacuum chamber. However the Peltier cell driver must be able to control the current in both flow directions and in this case is used the linear power amplifier controlled through the software controller implemented in NI LabVIEW as well as the goniometer controller.

The current flowing through the Peltier cell can be fairly high to achieve a required thermal transmission and due to the Peltier cell resistance is temperature dependent the Peltier cell power is highly nonlinear. Therefore to achieve a required performance of thermal stabilization system are designed two control feedbacks (the thermal and the power) controlled by the LabVIEW controller. Therefore the Peltier cell driver provides these features: the voltage and the current gain (sets the power), the current measurement (control the power), the temperature measurement (control the temperature) and the power source undervoltage lockout (control the ability of the power source).

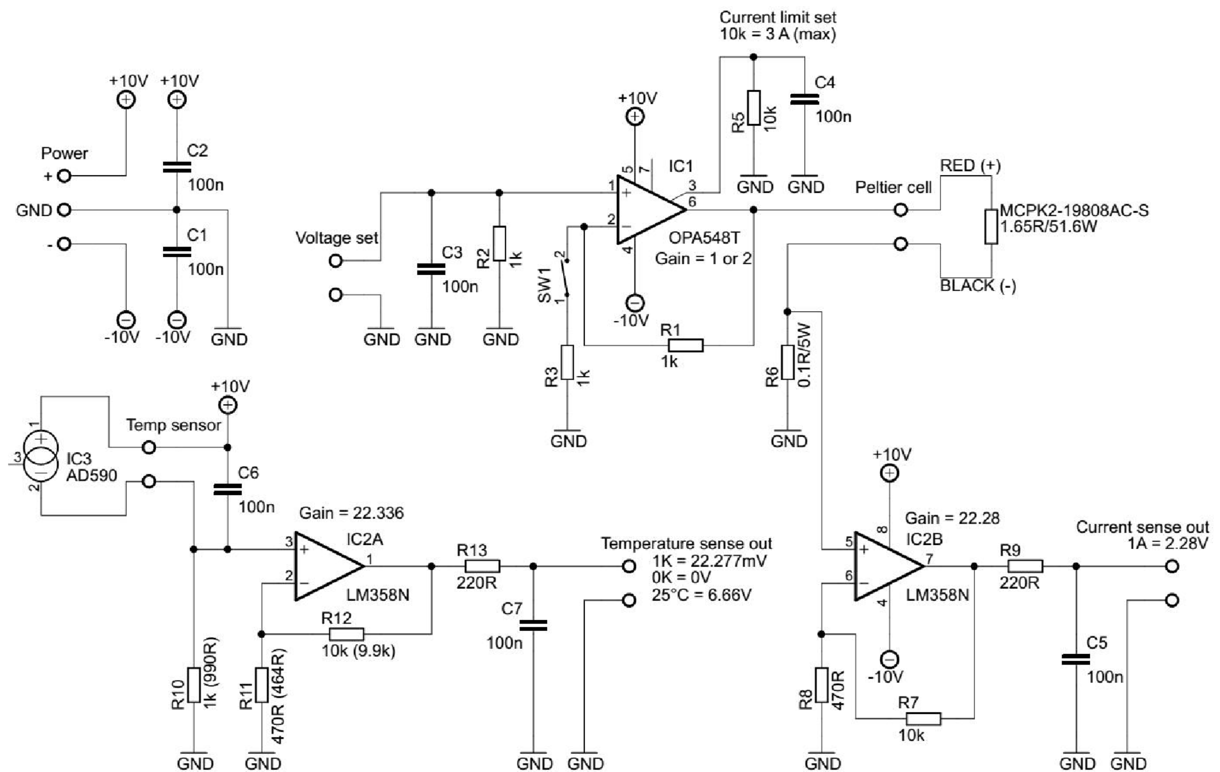

Figure 28: The wiring diagram of the thermal control driver

The figure 28 presents the designed wiring diagram of amplifiers for the Peltier cell driver, the temperature measurement and the current measurement. The Peltier cell power control is provided through the voltage setting magnified by the operational power amplifier OPA548. The amplifier gain is set to one therefore the amplifier magnifies only the current. However the amplifier gain can be increased by the resistor adding to twice.

The Peltier cell is behaving as resistance and since the voltage is applied the current starts to flow through the Peltier cell and produces the temperature difference. However the resistance of the Peltier cell is highly dependent on the temperature difference therefore the temperature changes of Peltier cell causes the changes of Peltier cell resistance. Moreover the amount of transferred heat depends on the electrical work (the electrical power) and not only on the voltage or on the current. Therefore the controller contains the primary power loop to control the Peltier cell power which is implemented as the current measurement of the power amplifier output provided by the voltage measurement at the shunt resistor ($0.1\ \Omega$). Then the voltage drop is amplified by non-inverting amplifier with gain 22.28.

The temperature measurement is provided by the temperature transducer AD590K which converts the measured temperature to the current which is flowing through the sensor. The sensor sensitivity is $1\ \mu A/K$ and the sensor has defined temperature range from $-55\ °C$ to $150\ °C$. The AD590K is calibrated to the nominal value $25\ °C$ with the nominal current $298.2\ \mu A$ and the accuracy of sensor is $\pm 0.5\ °C$. The sensor measurement current flows through the shunt resistor ($1\ k\Omega$) and the induced voltage drop is measured by the operational amplifier (neglected input current is $45\ nA$) and magnified by 22.336 gain. To achieve better temperature measurement accuracy were the values of the used resistors checked by Agilent multi-meter (accuracy ± 0.1 %) and these values are then used to the amplifier gain calculation and are also written to the wiring diagram (see the figure 28). The temperature measurement provides the secondary temperature control loop.

6.3 Thermal control setup

The tested device is mounted to the copper plate which is temperature stabilized by the Peltier cell through two copper heat pipes. The heat pipes provide heat transfer from the tested device to the aluminum base (cooler) or vice versa. The shape of the heat pipes can be slightly adapted to the shape of gyroscope front-en electronics (see figure 29).

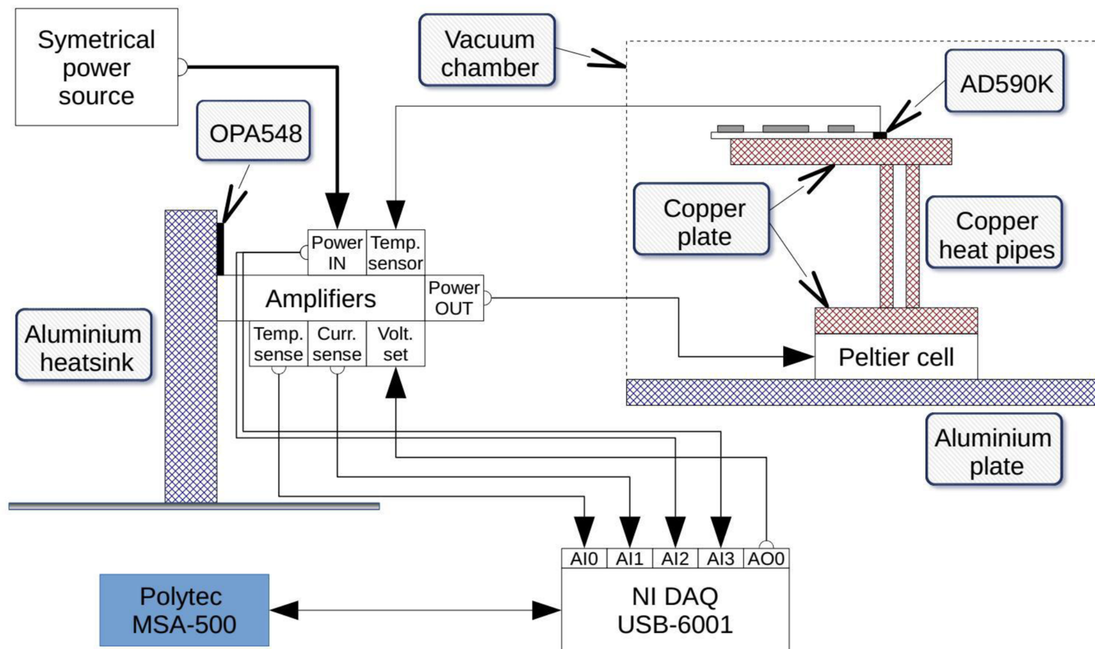

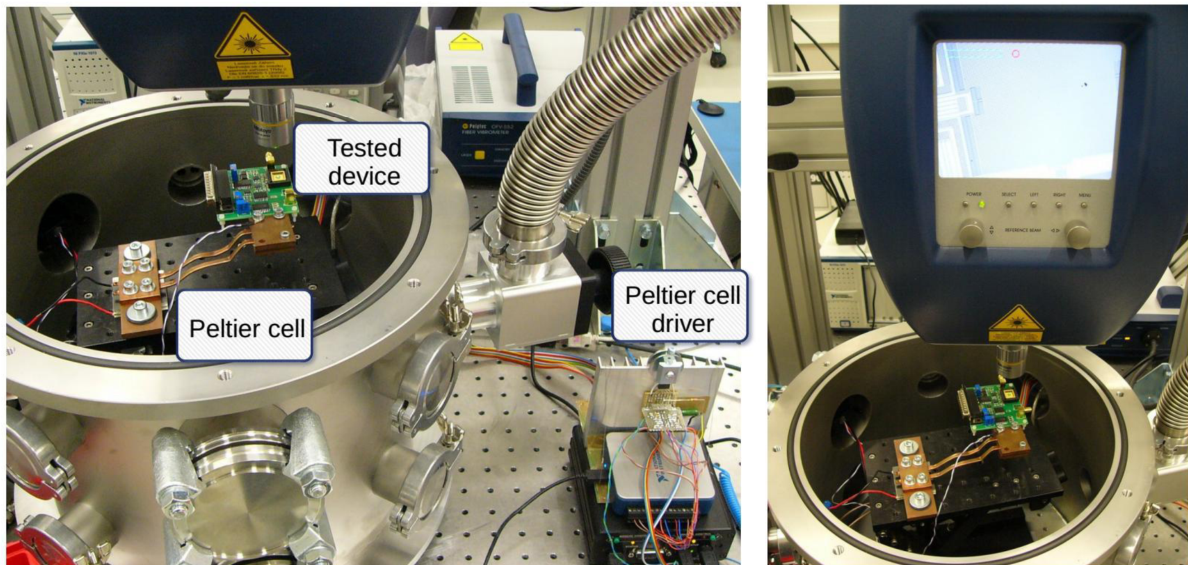

Figure 29: The thermal control setup (the block diagram and an illustrations)

The main component of the Peltier cell driver is the power amplifier (OPA548) in standard TO220 package. The OPA548 is mounted to the aluminum heat sink therefore the regulator is linear and its power dissipation can be in orders of watts. The amplifier power source must be symmetrical with minimal value $\pm 10\,V$ or higher. The minimal voltage is required to achieve the full-scale of the sensing amplifiers.

The temperature sensor is mounted together with the tested device to the copper plate which provides good thermal conductivity to temperature stabilization of the electronic components and also the gyroscope structure. The Peltier cell is mounted to the aluminum adjustable height platform which has the massive black color aluminum surface and provides good cooling capability of the Peltier cell in high vacuum. The adjustable height platform was also purchased from the Standa Company.

Figure 30: Adjustable height platform

As the analog signal frontend for the LabVIEW software is used the low-cost NI USB-6001 DAQ card which has sufficient properties for this type of controller. The card contains two analog outputs ($14\ bit$, $5\ kS/sec$ for all outputs) and four differential or eight referenced analog inputs ($14\ bit$, $20\ kS/sec$ for all inputs). The voltage ranges of the outputs and the inputs are the same with value $\pm 10\ V$ as well as the resolution with value $1.2\ mV$.

The ranges and the accuracies of the discussed thermal setup are:

- Temperature measurement: The AD590K range ($-50\ °C$ to $150\ °C$) produces the voltage range from $5V$ to $9.5\ V$ which is still in range of NI card. The temperature measurement accuracy is under $\pm 1\ °C$ at full temperature scale and depends on AD590 calibration ($\pm 0.5\ °C$), LM358 bias stability and NI card accuracy ($\pm 0.5\ °C$).
- Current measurement: Theoretical limit is over $\pm 4\ A$ which produces $\pm 9.2\ V$ however the current is hardware limited to $\pm 3\ A$ by OPA548. The current measurement accuracy is ca. $\pm 50\ mA$ and is highly dependent on the shunt resistor noise.
- Voltage adjustment: The voltage range is the same as the NI card range ($\pm 10\ V$) and if it is required can be hardware increased to $\pm 20\ V$. The voltage adjustment accuracy is under ±34 mV at full scale however the voltage drop at the shunt resistor must be compensated by the software controller.

6.4 THE SOFTWARE STRUCTURE OF THE THERMAL CONTROLLER

The controller is implemented in standard LabVIEW environment however the installation of the additional PID and Fuzzy logic toolkit is required. The secondary control loop (the master thermal controller) consists of an advanced PID controller which has implemented features as the filtration of derivative and set point value, set point range and nonlinearity compensation and advanced derivative part damping. The primary control loop (the slave power controller) consists of basic PI controller.

The controller is connected as the cascading controller therefore the slave controller sets the voltage to the Peltier cell, measures the current and control the Peltier cell power. The master controller sets the Peltier cell power, measures and control the temperature of the tested device. The slave PI power controller contains low integrative constant to suppress the fast power changes of Peltier cell and provides the power control especially in case the manual control of Peltier cell power is required by software.

The controller also contains the under voltage lockout system which periodically decreases the output power limit in case the voltage drop under $\pm 9\ V$ is detected. The voltage drop is usually caused by the current limitation in the laboratory power supply sources.

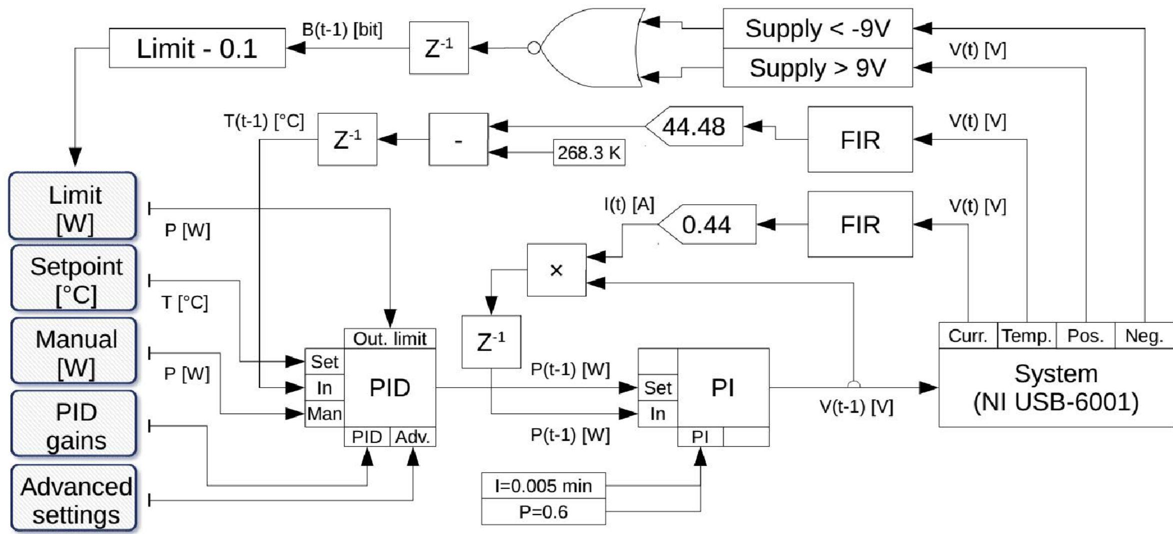

Figure 31: The block diagram of the thermal controller

The measured values (the temperature and the current) are filtered by FIR type low pass filter which suppresses the fast changes in measured values caused due to sampling and quantization. The filtered values (voltages) are adjusted by the gains and the offsets to obtain the system variables (the temperature and the current). The temperature sensor (AD580) is outputting the temperature in the Kelvin units which are transferred to the Celsius units due to absolute zero temperature subtraction. However the temperature sensor offset was calibrated by platinum thermometer and the overall temperature offset is $268.3°C$. The temperature and the current values are then calculated by the following equations:

$$\mathbf{T} = \frac{\boldsymbol{V_{IN}}}{\mathbf{22.304 \cdot 10^{-3}}} - \mathbf{268.3} \ \ [°\boldsymbol{C}] \qquad\qquad \boldsymbol{I} = \frac{\boldsymbol{V_{IN}}}{\mathbf{2.255}} \ \ [\boldsymbol{A}] \qquad \text{eq. (6.1)}$$

The slave power PI controller is outputting the voltage value which is setting the Peltier cell power. The power controller measures the power variable due to multiplication of the measured current and the set voltage. However to avoid the algebraic loop in the power controller there is implemented the one step digital memory which is storing the measured values and therefore the controllers are one step (sample) delayed behind the system. The sampling period of the thermo controller is software set to $25\ Hz$ and the controller dead time is $40\ ms$ however the controller dead time is negligible due to system time constants and delays.

The master thermal PID controller finally control the temperature of the tested device and there are implemented additional features:

- The output limit: limits the output (power) of the controller and avoids the power supply or Peltier cell overload.
- The under voltage lockout: in case the power supply voltage drops under 9 V in amplitude (the negative or the positive supply voltage line) the system starts to decrease the set power limit periodically than reach the zero. Therefore the system avoids the measurement error in the input amplifiers due to low supply voltage.
- Advanced settings: contains the derivative filters to avoid the very fast controller response due to derivative part of controller, the set point filter and the nonlinearity compensation to suppress the process variable overshoot.

6.4.1 The identification of the controlled system

The PID controller constants (gains) must be calculated in accordance to the system dynamics to achieve the required quality of control. There are plenty of identification methods to obtain the system parameters (e.g. state observers, Kalman filters, frequency response, approximation methods, etc.) in this case is used the step system response which is straightforward method to identify the most important system dynamics. The step system response is measured in $1.33\ Pa$ $(10\ mTorr)$ vacuum as the temperature response caused by constant Peltier cell power step.

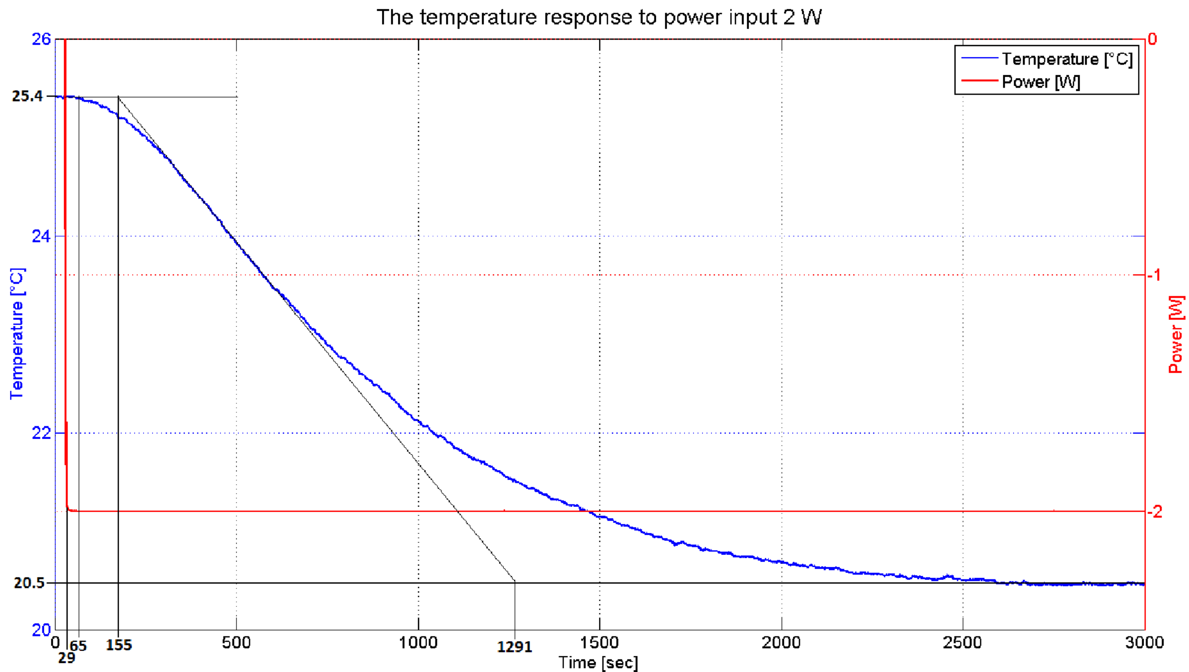

Figure 32: The system time response of temperature to power input 2 W in the vacuum (1.33 Pa)

The system step response curve is approximated by the linear dependence with intersection in inflexion point of the step response curve and then can be read out the time constants of the system. The linear approximation earmarks the important time constants of the system. The first part of the step response is the system delay time which is the no response time of the system since the input power step started. The second part is the system response time and the last part is the system rise time. The time constants of the thermal system then are:

- Delay time: $\tau_d = 65\ sec - 29\ sec = 36\ sec$ this time cannot be included to the system response time and also to the PID constants calculation.
- Response time: $T_u = 155\ sec - 65\ sec = 90\ sec$ is the intersection time of the approximation line and the starting temperature value.
- Rise time: $T_n = 1291\ sec - 155\ sec = 1136\ sec$ is the rise (or the decrease) time of the process variable (the temperature).
- Process gain: $K_s = \frac{\Delta T}{P_{in}} = \frac{25.4-20.5\ °C}{2\ W} = 2.45\ °C/W$ the process gain is calculated as the ratio of the temperature difference caused by constant power input.

For comparison of the thermal control system performance in the vacuum and in the normal ambient pressure there was also measured the system time response in normal ambient pressure. As the figure 33 presents the system time response in the normal pressure is more than twice faster as the response in the vacuum. However it could be caused by higher thermal resistance in the connections between the Peltier cell and the copper plate or the cooler therefore the dry heat conducting layer (graphite pad) is used.

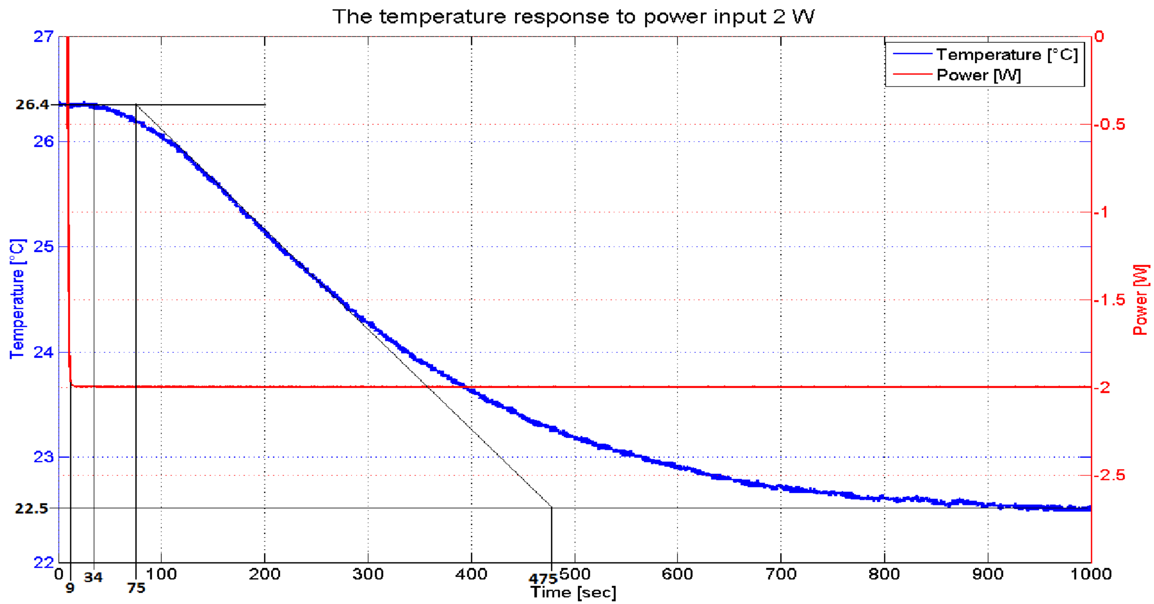

Figure 33: The system time response of temperature to power input 2 W in the ambient pressure (≈0.1 MPa)

6.4.2 The PID constants evaluation by Z-N method

The Z-N method is the experimentally based method for PID constants calculation due to the conversion table prepared by the J. G. Ziegler and the N. B. Nichols. The table is based on fundamental knowledge about control systems and presents the equations for calculation of the P, PI, PD or PID controller gains, inter alia, from the system step response characteristic. The PID controller contains three parts: proportional, integrative and derivative part and each part is defined by the gain and the time constant. However it can be simplified to one equation (6.2) of the PID controller with three values: the gain of the controller (contains all partial gains), the integrative time constant and the derivative time constant. These values can be simply referred to as the PID control gains or the PID control constants. In the LabVIEW controller is used the conventional PID controller equation:

$$\boldsymbol{F_C(s) = K_C(1 + \frac{1}{T_I s} + T_D s)} \quad \text{eq. (6.2)}$$

K_C Gain of PID controller
T_I Integrative time constant
T_D Derivative time constant
s Laplace operator

The table assembled by Ziegler and Nichols is presented in [13] and contains the equations (6.3) to calculate the PID gains from the system step response characteristic shown in figure 32. The equations are:

$$\boldsymbol{K_C = 1.25\frac{T_n}{T_u \cdot K_s} \qquad T_I = 2T_u \qquad T_D = 0.5T_u} \quad \text{eq. (6.3)}$$

Then the initial values of the PID gains used for tests in vacuum chamber are:

- $K_C = 1.25\frac{1136}{90*2.45} = 5.15$
- $T_I = 2 \cdot 90 = 180\ sec = 3\ min$
- $T_D = 0.5 \cdot 90 = 45\ sec = 0.75\ min$

The PID controller gains are slightly coerced during the system tests to achieve better performance of thermo control system. The thermo control system performance tests are placed in chapter 7.3.

7 THE MEASUREMENT SYSTEM

This chapter presents the developed LabVIEW application for control the designed measurement chain to test the MEMS gyroscopes and therefore the application is named the Measurement System. The Measurement System contains the software foundations for control the goniometer stages (discussed in chapter 5), the topography measurement (discussed in chapter 4) used for slope compensation of the tested device and the thermal control system (discussed in chapter 6) used for temperature stabilization.

The LabVIEW project is also named the Measurement system.lvproj and it contains one main Virtual Instrument block (VI) with the mane Measurement system.VI. The application program is compiled as hybrid type of state machine, with structure shown in figure 34, which combines the super loop architecture and the state machine programming techniques. In a classical state machine is a sequence of cases which are executed one after another and are switched each other as a chain. The Measurement System application uses the event structure which is timed in the main while loop and in every loop iteration the event structure is waiting $25\ ms$ for user activity at front panel and if the user activity is not detected, the event structure executes the specified timeout case with special (none) sequence of commands. However in case the event structure detects an activity at front panel (triggering the button typically) there is selected the relevant part of the code which is corresponding to the appropriate button action. Importantly the main feature of this hybrid state machine is the idle mode of the application where only the required part of code is executed.

To better user friendliness is the application divided to the several tabs and each tab contains its own part of code including the timeout code (see figure 34). Therefore if one particular panel is selected the code of the other panels is not executed except the main timeout case in the event structure. The specific code parts are discussed in the next text.

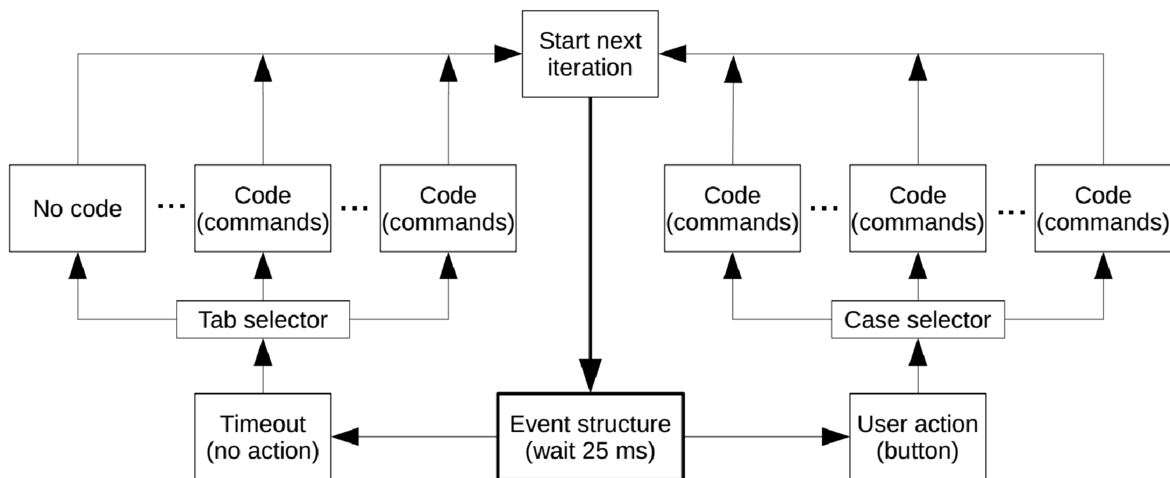

Figure 34: The flowchart of the LabVIEW application (the Measurement System)

7.1 LABVIEW CONTROLLER FOR THE GONIOMETER STAGES

The LabVIEW controller communicates with the hardware controller via USB interface and the controller drivers must be installed on the operator PC. Then the commands can be sent to the controller via virtual serial port (COM) which is now mapped in the device manager. For this controller is available the LabVIEW library which contains basic commands (functions) for control the movement of the stepper engines and reading the controller status for example: Move right, Move left, Get status or Move to position in steps or in user defined units.

The Measurement System application requires the standard 32 bit version of the LabVIEW software 2013 or later, also requires the PID and Fuzzy Control Toolkit [14] and also requires the NI myDAQ drivers [15] as the additional software downloaded from NI support pages. If the application is properly opened, the window of the main panel shown in figure 35 is visible. The "Main panel" of the application is mostly devoted to the goniometer controller however also contains the main Exit button which is important to properly termination of the application and the connected hardware (especially the goniometer controller and the thermo driver) otherwise the communication ports can stay unclosed.

7.1.1 The goniometer movement commands

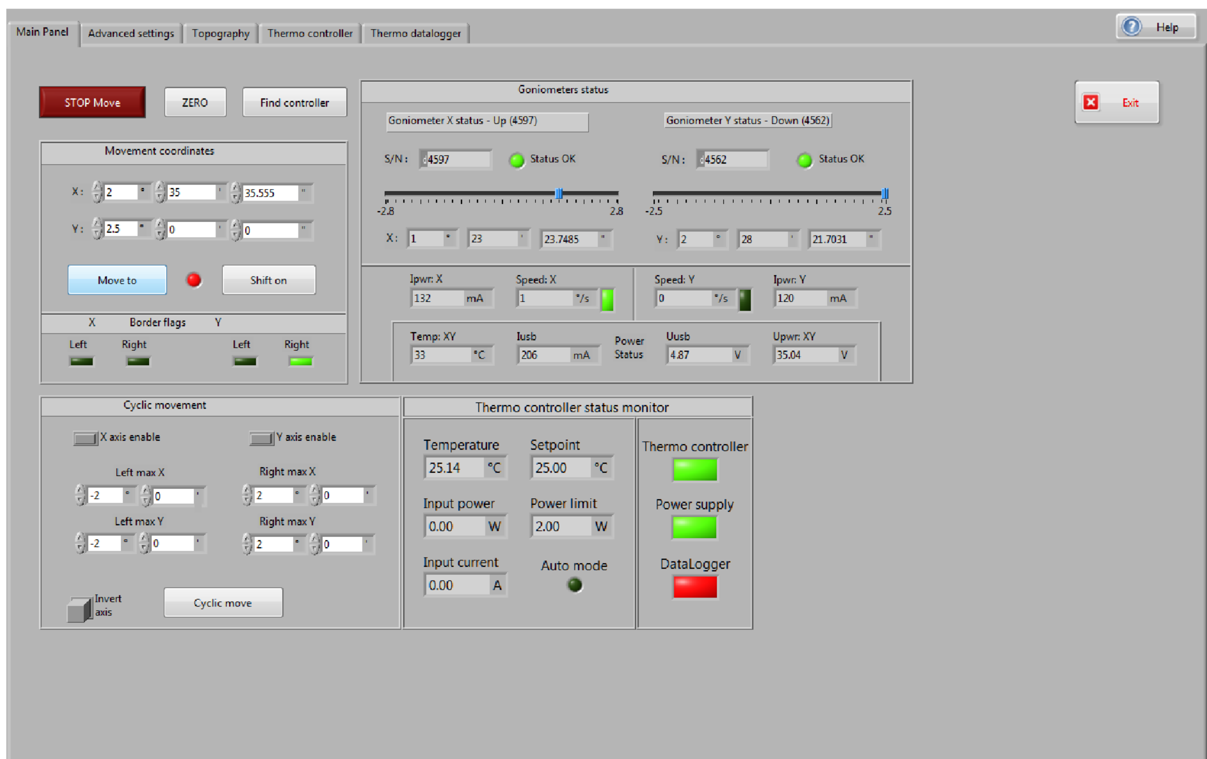

Figure 35: The main panel of the Measurement System

The middle section of the "Main panel" is devoted to the goniometer status there are the controller status indicators which signalizes the goniometer controller is properly connected. The linear indicators present the actual position of the goniometers however this value is also presented numerically bellow in the units of degrees. There is also presented the actual speed of the goniometers in degrees per second and the small green square indicator announces the appropriate goniometer reached the speed setpoint set in the "Advanced settings" tab. The others indicators present the additional controller information as the engine winding current, the controller supply voltage, the controller temperature and also the USB interface power status. The code to read the goniometer status is inserted to the timeout loop therefore the indicators are refreshed every $25\ ms$ however just if the main panel tab is selected which is in accordance with figure 34.

The text boxes "S/N" in the goniometer status section monitors the actual serial numbers of the each controller axis. These numbers are not important for the operator however there should be the unique numbers which are written in the labels above the text boxes. When the application is starting, the library function automatically starts to search the available controllers and returns the serial numbers of each axis in random order. Unfortunately the two goniometer stages are slightly different (see the chapter 5) and the controller axes are automatically sorted by the serial numbers to avoid the axis confusion. In case the goniometer setup is rearranged the numbers of controller axis can be helpful.

The status information is read out by the library VI with the name: "get_status_calibrated.VI." The controller is able to recalculate the position values for the stepper engines to user defined units instead of the dedicated steps and moreover the controller also supports the microstepping technique wherein each step is divided to 256 microsteps. Hereby the controller can control the stepper engines inside the one of the dedicated steps. To activate this ability must be in the LabVIEW each goniometer position command (included the get status command) connect together with the calibration cluster which contains the calibration data (the angle per step resolution) and the microstep mode. This cluster is compiled in dedicated VI named "get calibration.VI" which prepares the data for the main command VI. The calibration data are available in the main data cluster which stores all of the program data (see the figure 36).

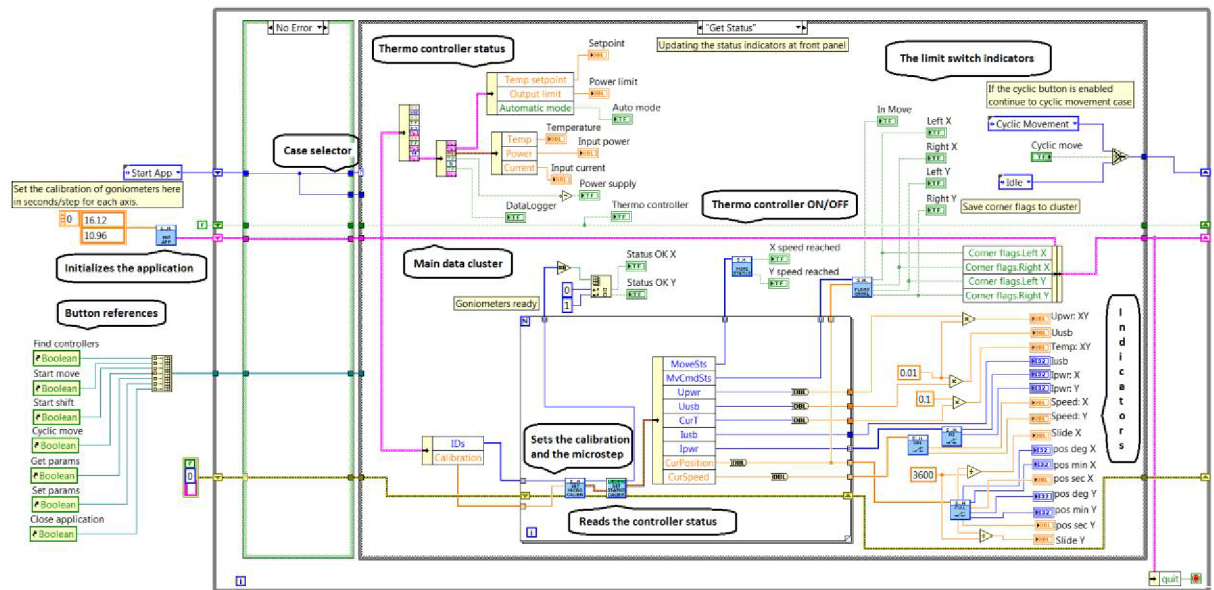

Figure 36: The LabVIEW code demonstration for reading the goniometers status

The program code is situated to one case structure in the while loop which is similar to classical state machine however after the case (program block) is executed the case structure is swapped to the idle case (see the blue case selector in figure 36) where the event structure is placed and control the flow of the code according to figure 34. The ping cluster visible in the code is the main data cluster which contains the calibration data for each goniometer (its order corresponds with the main panel, the first is X and the second is Y goniometer). Due to this data cluster all of the program data are available in each case and can be updated for the next iteration. The main data cluster contains: the goniometer position for the next move, the goniometer limit switch indicators, the topography data, the thermo controller data and also the goniometer calibration data.

The left section of the "Main panel" (see the figure 35) is devoted to the goniometer movement controller to the manual control of the goniometers. The upper red button is used to immediately stop the goniometer movement in emergency situations however the goniometers are stopped hardly (without slowdown) and the stepper engines can lose the step and the actual position is lost. Moreover too frequent using of the stop button can wear out the goniometer gears. The other button is used to reinitialize the goniometer controller in case the controller is not loaded during the application startup process. The zero button is used to set the actual position of the goniometers as the new zero position of the goniometer trajectory and the actual goniometer rangers are also coerced by the new zero values.

The boxes bellow are used to set the angle to the goniometers in X axis (the upper goniometer) and in Y axis (the bottom goniometer) and after triggering the "Move to" button the event

structure in the application code stores the movement coordinates to the main data cluster and switches the movement case with corresponding code section. There are the movement data loaded from main data cluster and the library VI sends the coordinates to the goniometer controller and switches the application to the idle mode. The “Shift on” button works similarly to the “Move to” button however the movement coordinates are added to the actual goniometer position.

The angular coordinates can be set in integer or in floating point format therefore the statements as: $1.5°$, $1°30.50'$ or $1°30'30.33''$ are allowed however the application recalculates the values to seconds in floating point and sends them to the goniometer controller. The controller recalculates the values again to the steps and microsteps, sets the goniometers and then the application in idle loop reads the set coordinates from the controller in the “degrees minutes seconds” form and shows them at the maim panel.

The red light between the movement buttons (see the figure 35) signalizes the goniometers are moving. The square green indicators below the buttons signalizes the activation of the hardware range limitation (the maximum angle) of the goniometer stages and the indicators in the application have the same function as the indicators at the front panel of the controller box.

The bottom left section of the “Main panel” (see the figure 35) is devoted to the cyclic movement of the goniometers. However the controller is “deterministic,” each command sent to the controller must be fully executed or aborted before next command execution will start. For example: if the coordinates are sent to the goniometer controller, the controller is waiting until the goniometer reach the position and any next movement command is stored in controller memory and will be executed thereafter.

The cyclic movement algorithm is triggered by the “Cyclic move” button and the main event structure stores the angular range set in the boxes at front panel (see the figure 35) to the main data cluster. Then the event structure switches the movement part of code, the coordinates are sent to the controller and there are executed. During the command execution process the application is switched to the timeout loop which is periodically checking the goniometer position and if the goniometer is reaching the set position (or the limit flag indicates the overage) the timeout loop is extended by the movement code and the coordinates of the opposite position are sent to the controller. Due to the controller memory stores the new commands the goniometer movement is cyclic and smooth with ascending and descending ramp trajectory. The cyclic movement is ended by unlatching the “Cyclic move” button and then the event structure sends the zero position to the controller.

However during the cyclic movement the event structure is still waiting for user activity and the program flow can be easily interrupted by user. Therefore the other movement buttons and the tab selector are disabled during the cyclic movement is in progress due to button references visible in the figure 36. The cyclic movement can be certainly interrupted by the red “Stop” button which immediately stop the goniometers and the cyclic movement is forced to end.

The two small switches above the cyclic move boxes are used for disabling or enabling the appropriate controller axis (the goniometer) which will be skipped from the cyclic movement. The switch with label “Invert axis” is used for inverting the axis movement and if the button is latched the goniometers starts to move in opposite directions which is useful in case the goniometers are installed linearly to the one axis to increase the angular range.

The last middle bottom section of the “Main panel” (see the figure 35) is devoted to monitoring the thermo controller status. The thermo controller can fully operate with goniometer controller including the goniometer cyclic movement. There are indications of: the thermo controller is turned on or off, the thermo data logger is turned on or off, the power supply status (the undervoltage lockout system), the automatic control status, the actual power of the Peltier cell and the power limitation and certainly the device temperature and the temperature setpoint.

7.1.2 The Advanced settings tab of the application

The tab named “Advanced settings” (see the figure 37) is devoted to additional application setting. The left section contains the special function which finds the center of the goniometer trajectory, the middle section contains the function for reading and setting the goniometer engines speed [°/sec], acceleration [°/sec²] and deceleration [°/sec²] and the right section contains the thermo trajectory function which can be used for control the device temperature over user defined point by point trajectory.

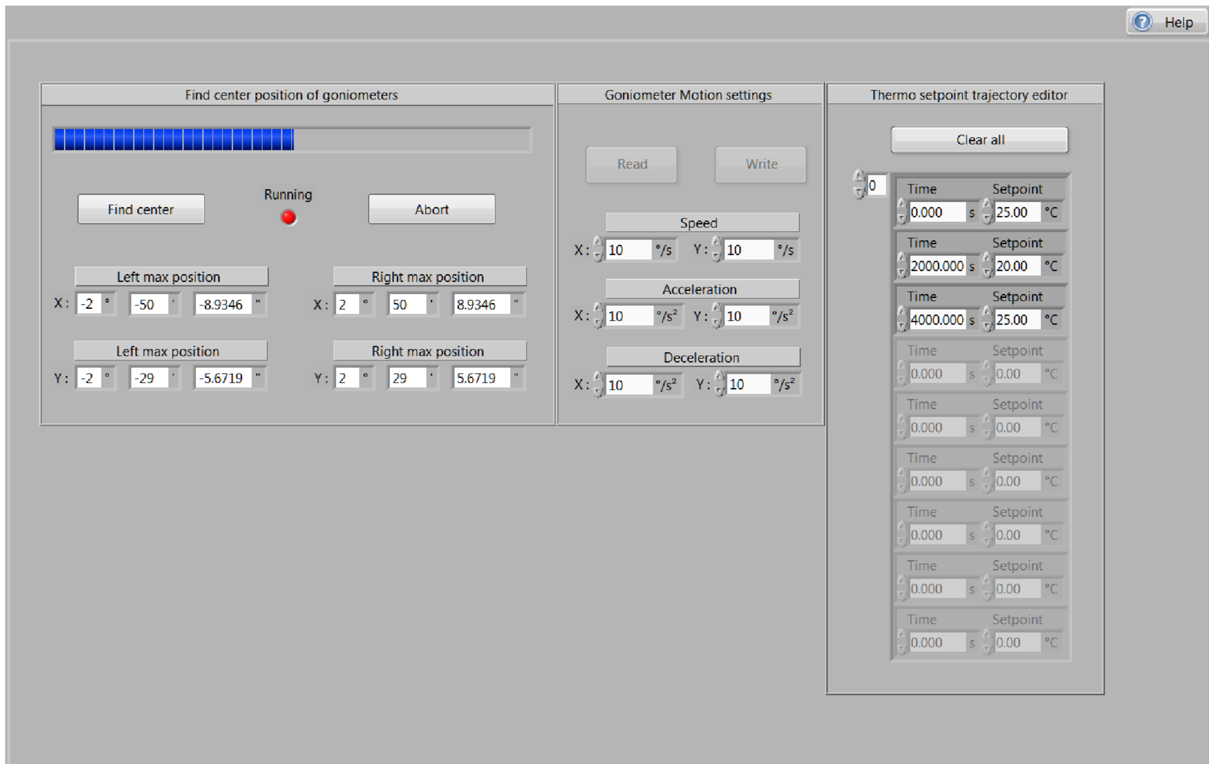

Figure 37: The Advanced settings tab of the Measurement System

As mentioned the goniometer controller contains a FLASH memory which stores the control data including the last goniometer position independently of the controller power supply and if the controller is turned on again the information about the last goniometer position is still available. However in some cases is needed to recalibrate the center position of the goniometers especially in case the stepper engines have lost the steps typically in overloaded conditions (too hard acceleration or deceleration). Due to the function “Find center position of goniometers” can be the center of goniometer trajectory recalibrated and therefore the zero position in the main panel will be the center of trajectory and the maximum ranges of the goniometers will be found. Unfortunately the center of goniometer trajectory certainly is not in the orthogonal orientation with respect to the Polytec measurement head.

The code section of the “Find center position” function is located in the “HOME” case and is selected by the main event structure due to triggering the “Find center” button. However the function is realized as a small state machine considering the function complexity and therefore the “HOME” case contains separated structure of cases which are selected by another case selector stored in the main data cluster. However the find center function still works with the main event structure and its timeout loop in waiting periods and therefore the timeout code sections (especially the thermo controller) are still executing.

The operation principle of the Find center position function is similar to the cyclic movement. Firstly is sent the command for move to the right direction (this is the library function). Both of the goniometers are moving with internally defined speed to the right direction until they trigger the limit switches which are scanned by the program. Then the maximal right angle is storied

and the command of the opposite movement direction (to the left) is sent to the controller and then the left maximal angle is also stored. This two limit positions are subtracted and the difference is divided by two. This absolute position is the wanted center of the trajectory and are sent to the controller. The library function (the “Zero” command) saves the new position to the goniometer controller as the zero position of the trajectory. In the end of the Find zero position program are the maximal positions coerced by the new center position and are loaded to the indicators in the front panel therefore they presents the maximal achievable angle of the each goniometer. The center calibration process is signalized by the progress bar and takes around 30 seconds; in emergency situations can be aborted by the “Abort” button.

The goniometer motion setting section is used to set the specific speeds of the stepper engines to the goniometer controller. However these values are not stored in the controller memory and must be reloaded after each controller restart. The “Read” button triggers the event structure which selects the library function for reading the speed setting from the goniometer controller and shows it in the boxes. The operation of the “Write” button is similar and the speed setting from the boxes is loaded to the goniometer controller. Importantly the acceleration and deceleration values are limited by the stepper engines and the maximum values are approximately $25\ °/sec^2$ where the engines starts to lose the steps due to rotor dynamics. The speed value has the maximum achievable speed approximately $15\ °/sec$ due to the trajectory length.

The thermo trajectory editor is used to creating the user defined temperature trajectory for the thermo controller. Each pair of the boxes (the time and the temperature) is used as the one point of the trajectory and the sections between the points are then approximated by the linear function. The number of trajectory points is unlimited as well as the duration time of the overall thermo trajectory. The trajectory points can be deleted by deleting the numbers in the appropriate row or by the “Clear all” button which clears all of the trajectory points. The trajectory editor code is located in the separated VI named “PID Set point Profile” which is taken from the PID and Fuzzy Control Toolkit library.

7.2 LabVIEW APPLICATION FOR THE TOPOGRAPHY MEASUREMENT

As mentioned chapter 5.3 there are reasons to align the tested device surface with respect to Polytec measurement head which is needed to achieve good accuracy of the out-of-plane measurement. The Polytec MSA-500 contains the topography measurement system which is the way how to achieve this. However the Polytec MSA-500 is very sophistic and complex system and therefore it uses its own acquisition software which is not compatible with the LabVIEW software. However the Polytec software is able to measure the topography surface and export the data to the matrix form. Each number of the matrix represents the Z axis heights of the measured pixel. The maximal resolution of the scanning camera is $1400 \times 1000\ pixels$ therefore the matrix has $1\ 400\ 000\ numbers$ in single precision. The exported matrix is then loaded to the “Measurement System” application and it automatically aligns the surface of the tested device to approximately perpendicular orientation with respect to the Polytec measurement head.

7.2.1 The tested gyroscope sample

As the tuning fork MEMS gyroscopes designs developed by Honeywell International s.r.o. are confidential a MEMS gyroscope based on the publicly available design is used for demonstration purposes of the thesis. The gyroscope design is based on the publicly available design published in Ph.D. thesis [16] by Said Emre ALPER.

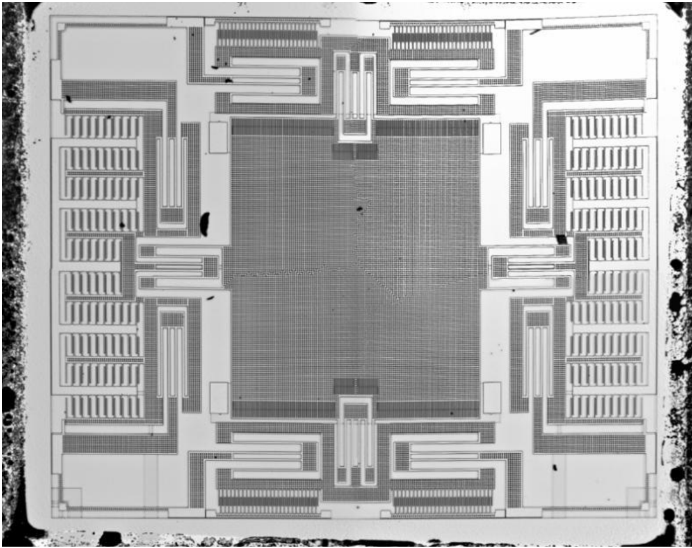

Figure 38: The Honeywell developed gyroscope design

The tested sample of gyroscope design is a single proof mass with double decoupled frame free topology design (see the chapter 3.1.2). The design is, however modified by Honeywell (sense, drive combs dimensions, beams and springs dimensions, and the resonance frequency) to achieve similarity with the gyroscope designs developed by Honeywell International s.r.o. Aerospace Advanced Technology Europe.

7.2.2 The Polytec MSA-500 topography measurement

The tested device (gyroscope) is mounted to the goniometer setup (see the chapter 5) and then the Polytec optic is focused to the gyroscope surface (the proof mass typically). The surface of the uncovered gyroscope is measured by the TMS software which is presented in the figure 39. The TMS system contains multitude of setting which must be set before the measurement starts, importantly it is the measurement height range in Z axis which must be sufficient to containing entire gyroscope structure (typical range is $\pm 50\ \mu m$ maximal range is $\pm 122\ \mu m$, the exposure time which sets the optimal brightness of the measurement light (typical value is $1/2000\ s$) and the threshold which should be as lowest as possible than it starts to increase the brightness changes noise in the measurement due to high steps in the sample heights (typical value is 10).

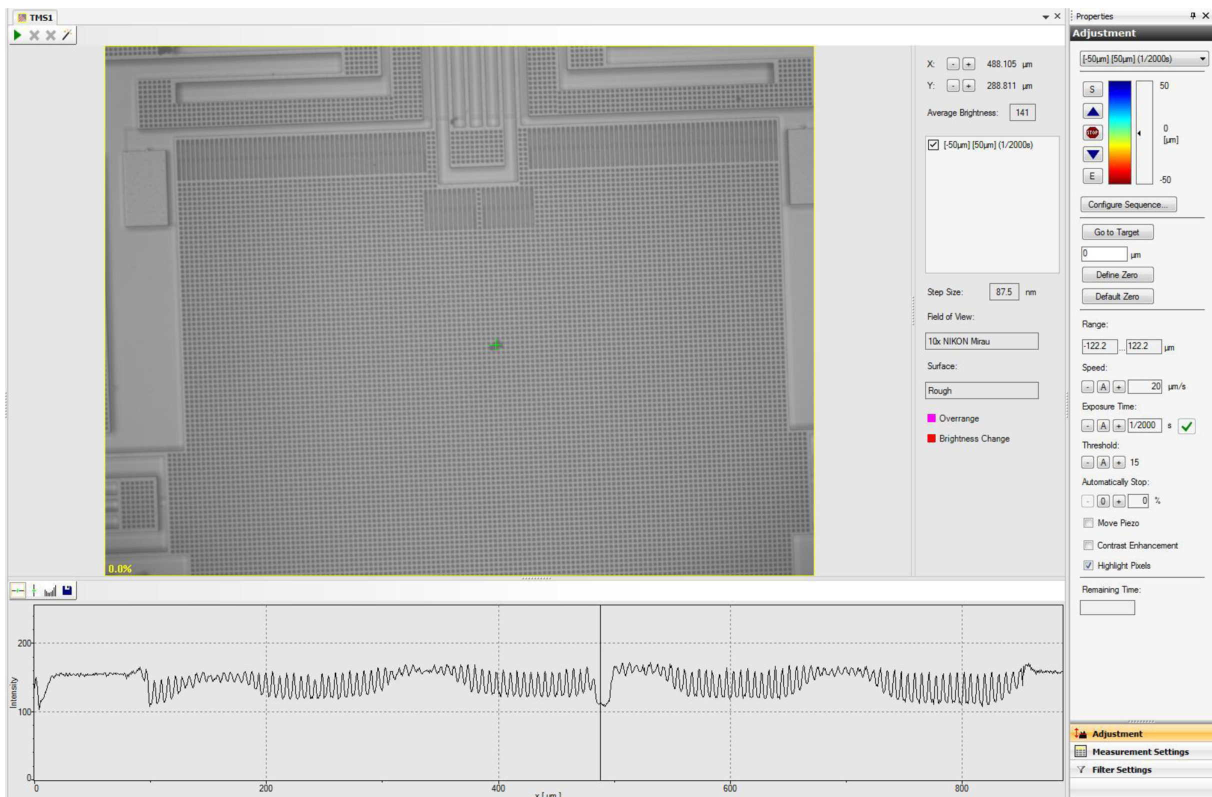

Figure 39: Example of the topography measurement by the TMS software

After the topography measurement ends the TMS software automatically starts the post-processing and shows the colored topography surface of the tested device. In the TMS menu bar can be selected the option: export to ASCI table and the system creates the TMSdata.txt file which contains the matrix of double precision topography data. The resolution of the scanned surface is $1400 \times 1000\ points$ and due to used lens (10X) it makes the scanned surface dimensions approximately to $860 \times 660\ \mu m$ and the size of one point is approximately $637 \times 637\ nm$.

7.2.3 The topography map in the LabVIEW application

The path to the TMS data file must be set to the textbox in the left upper corner however the file path can be also selected by the system explorer due to the button with the folder symbol. The “Read” button triggers the event structure and the sub VI starts to read the TMS data file.

However it is a text file and as such has the numbers presented as the strings which are then converted by the application to numbers. Unfortunately there is a decimal mark convention conflict therefore the EU is using the decimal comma and the USA is using the decimal dot. Both systems (the Polytec and the LabVIEW) are automatically prioritizes the decimal marking due to the operating system localization. Therefore the application must recognize the actual decimal mark convention and then ensure the appropriate decimal mark conversion before the string to number conversion starts. This process is provided by the code section in the VI named “Read TMS data” which stores the TMS matrix to the main data cluster.

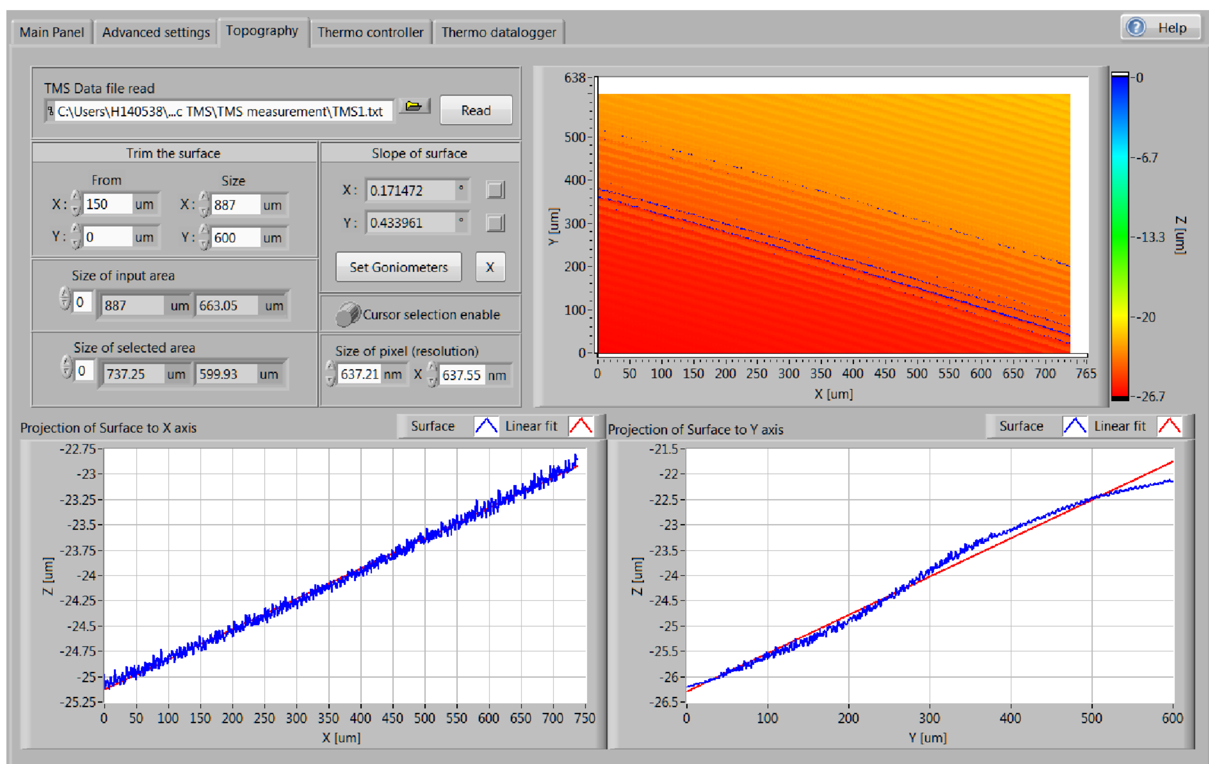

Figure 40: The LabVIEW application tab 3 - the topography measurement (no slope compensation)

The topography surface exported by the Polytec TMS system should be now visible in the right section of the topography tab panel and the data correctness of the measured surface can be checked. For better user friendliness the TMS matrix dimensions (points) are recalculated to the metric dimensions in μm. The calculation is provided by the VI named “Subsurface select” and the VI is also capable to sub select the input matrix and trim the surface by the indexing in the metric units (μm). The recalculation is carried out due to the topography resolution which is determined by the Polytec TMS system and especially by the topography lens (the default value is visible in the figure 40).

The “Trim the surface” section (see the figure 40) is used to focus the investigated surface (usually the proof mass of the gyroscope) and then the focused part of surface will be aligned by the goniometers. To trim the surface set the point of the origin and the length of the selected surface in μm in both axes. The boxes below presents the initial size and the actual size of the surface. The trimmed surface is visible in the topography graph in the right upper side of the window (see the figure 40).

The two graphs at the bottom of the window (see the figure 40) presents the projections of the selected surface to the X and to the Y axis. The projected surfaces (the curves) are then fitted by the linear dependences in each axis due to least square approximation method. The projected curves are calculated by averaging the appropriate columns over the axis range. Therefore the 1400×1000 points surface is averaged the two projection curves and the X axis curve has 1400 points and Y axis curve has 1000 points. The averaging algorithm can be skipped by the “Cursor selection enable” switch and the projection curves are now selected manually by incision of the topography graph due to selection an appropriate row and a column in the topography matrix.

The topography part of the application is controlled by the same main event structure as well as the goniometers however the topography part of code is slightly computationally intensive and compute this part of code in timeout loop is wasting of processing time. Therefore this part of code is computed only in case the user changes some value at the front panel due to the main event structure is also checking the status of the controls at the front panel and not only the buttons. Hereby the front panel is refreshed only if it is required by user and the timeout loop can be almost empty.

The gyroscope surface slope is obtained from the slope of the fitted lines in X and in Y axis and the angles are presented in the boxes at the middle of the topography tab panel (see the figure 40). The angles are calculated by the arctangent of the fitted line slope and it is converted to degrees units. The “Set goniometers” button automatically compensate the surface slope by setting the appropriate angle to the appropriate goniometer (the correction of angle). If the angles are properly sent to the goniometer controller the topography data are now useless and they are deleted from the main data cluster and frees approximately 6 MB from the system memory. However the data can be reloaded in the topography tab again. During the goniometers reaches the new position the small code part in the topography timeout loop is activated and waiting until the movement ends. Then the main panel is automatically selected and the new angles are visible as the actual goniometer positions.

The centering process can be repeated several times to achieve higher accuracy of the aligned surface with perpendicular orientation to Polytec measurement head. The maximal accuracy is usually achieved in third iteration of the centering process. The application also allows the angular compensation only in one axis if it is required by circumstances. The appropriate axis selection is provided by the square switches next to the slope angle boxes in the middle of the topography panel (see the figure 40).

The goniometer setup has variable installation setting and can be installed variously especially in the horizontal plane (see the block diagram of goniometer setup in figure 26). However the horizontal orientation must be consistent with the LabVIEW application for properly angular compensation. Therefore the application accepted four fundamental horizontal orientations which must be selected by user before the angular compensation process will start. The orientation setting between the Polytec measurement system and the goniometer setup is selected using the “X” button in the topography panel (see the figure 40) and the window, shown in figure 41, will pop up.

In the new window (see the figure 41) are marked two horizontal coordinate axis (the X and the Y) which are corresponding with coordinates in Polytec topography system and also in the exported topography map. In a nutshell, the X axis is parallel with the monitor at the Polytec measurement head. Hereby in this window can be easily recognized the orientation due to the marks on the goniometer engines and the correct orientation can be then selected by the green buttons. The selected orientation is saved to the attached binary file located in the application directory and for another angular compensation process will be used the last goniometer orientation. This function (VI) is controlled by the main event structure and the case named "Change the orientation." If the file with goniometer orientation is not found or is corrupted, this VI returns an error and the user is asked to set the new goniometer orientation.

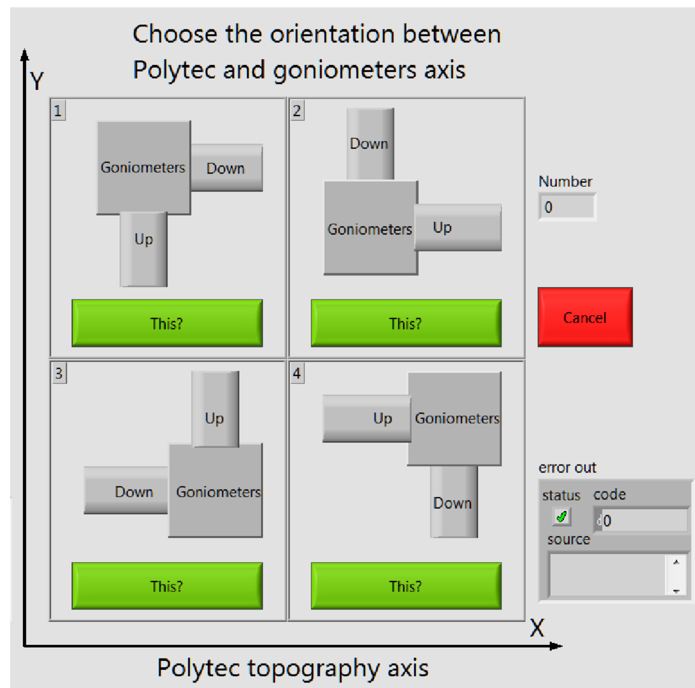

Figure 41: The goniometer setup orientation settings

7.2.4 The perpendicular aligned surface of the tested device

The first topography measurement and goniometer angular adjustment provides relatively good angular compensation performance; in the X axis is angular slope 0.001° and in the Y axis is angular slope 0.12° these values are measured by second topography measurement. The second iteration of angular compensation process and then the third topography measurement provides the angular compensation performance presented in the figure 42.

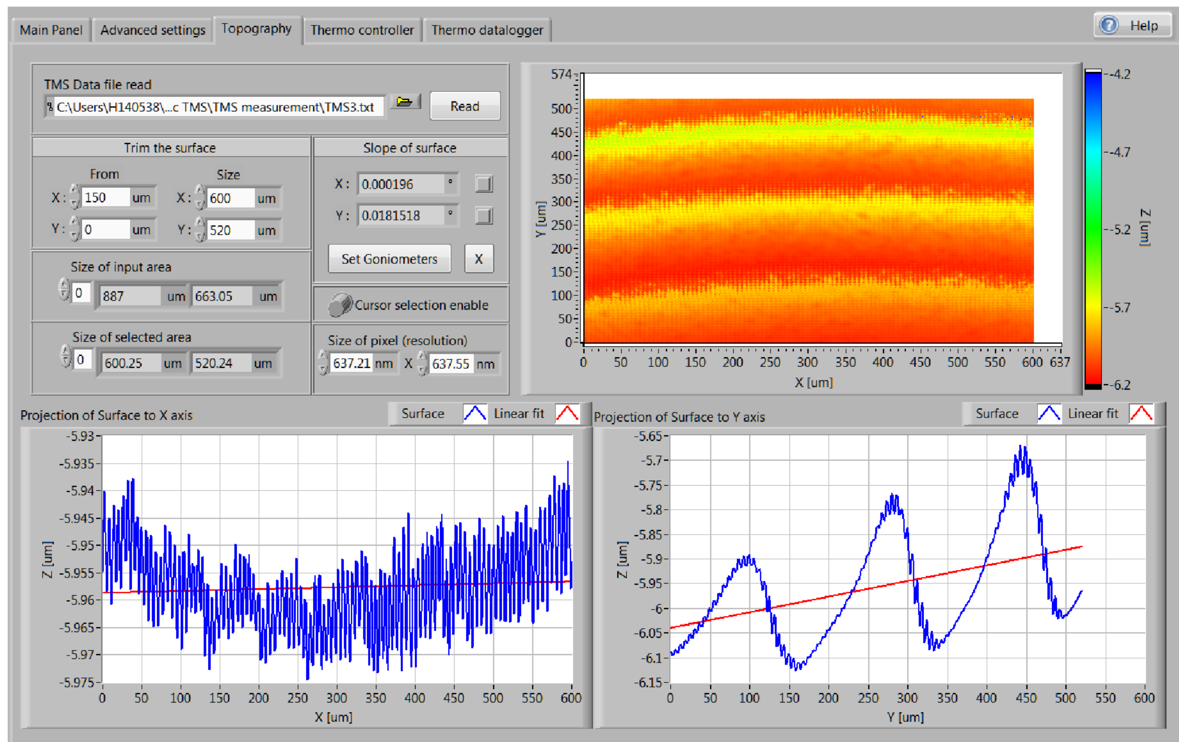

Figure 42: The third topography measurement of slope compensation process

The third and the final iteration of the angular compensation process is presented in figure 42. There is achieved the maximal resolution of the topography measurement and goniometer adjustment system. In the X axis is visible only the residual noise (slope $0.0002°$) of the topography measurement with amplitude approximately $30\ nm$ which is the maximal accuracy of the topography system on a rough surfaces (gyroscope proof mass perforation). In the Y axis are visible large waves which are caused mostly by the mechanical oscillation of the Polytec head stand due to its less stiffness in this axis. The linear approximation in the Y axis shows the residual angular slope approximately $0.018°$ which is almost two orders of magnitude worse than in the X axis.

However another iteration of the angular compensation process do not bring the better accuracy and the system starts to oscillate around the accuracy presented in previous paragraph. In some cases can be the axis disabling feature used to achieve higher accuracy in one axis especially in the Y axis to suppress the mechanical oscillation of the measurement head. All of the topography measurements are exported to TMS files (matrix) and can be also loaded by the application as a presentation of the alignment process. The TMS files are located in the application folder included on CD in annex.

7.2.5 The cursor selection feature of the topography tab

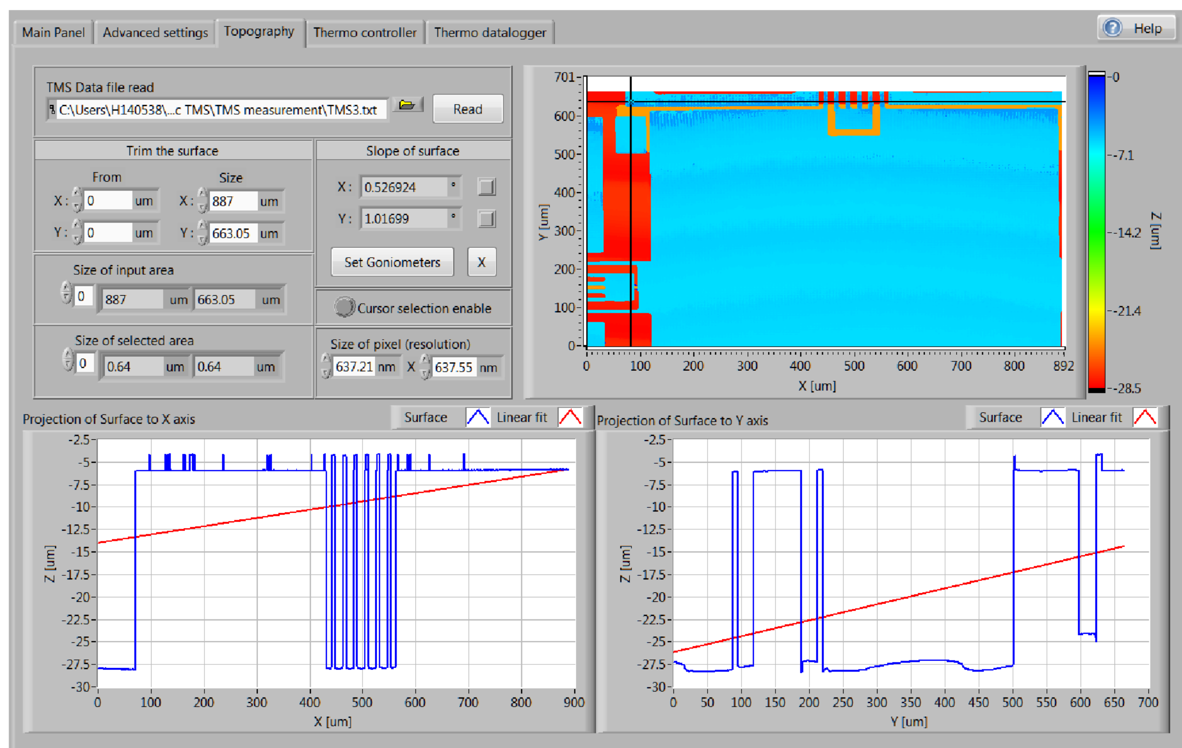

Figure 43: The topography tab - the incision by cursor selection feature

The cursor selection feature can be used also to the angular compensation process. The cursor incise the topography surface at the specified point as shows the X incision graph and the Y incision graph (see the figure 43). However the cursor tool decreases the overall accuracy of the angular compensation process due to selection only the one pixel row (column) of the topography map instead of a whole surface. On the other hand, the cursor tool can be useful to align the specified point or the small area of the surface.

Moreover the cursor tool can simply show the incisions of the gyroscope surface and especially the beams, the anchors and the depth of the substrate material under the proof mass (see the figure 43). Hereby the cursor tool can be used to detect the gyroscope structure defects.

7.3 The LabVIEW thermo control system

This part of the LabVIEW application provides the temperature stabilization of the tested device. The application is implementing the thermo controller setup presented in the chapter 6.2 and the LabVIEW thermo controller presented in the chapter 6.3. The thermo controller is placed as the sub VI (function) to the timeout loop of the main event structure (see the figure 34 in chapter 7) and hereby the controller is running in a superloop with sample period $25\ ms$.

The thermo controller uses the Peltier cell powered by the power amplifier and controlled by NI USB-6001 data acquisition card connected via USB. The thermo controller can fully operate together with goniometer controller and moreover the goniometer hardware controller contains the USB HUB which allows the controllers can be connected serially and uses only one USB connector in the host PC.

7.3.1 The Thermo controller tab

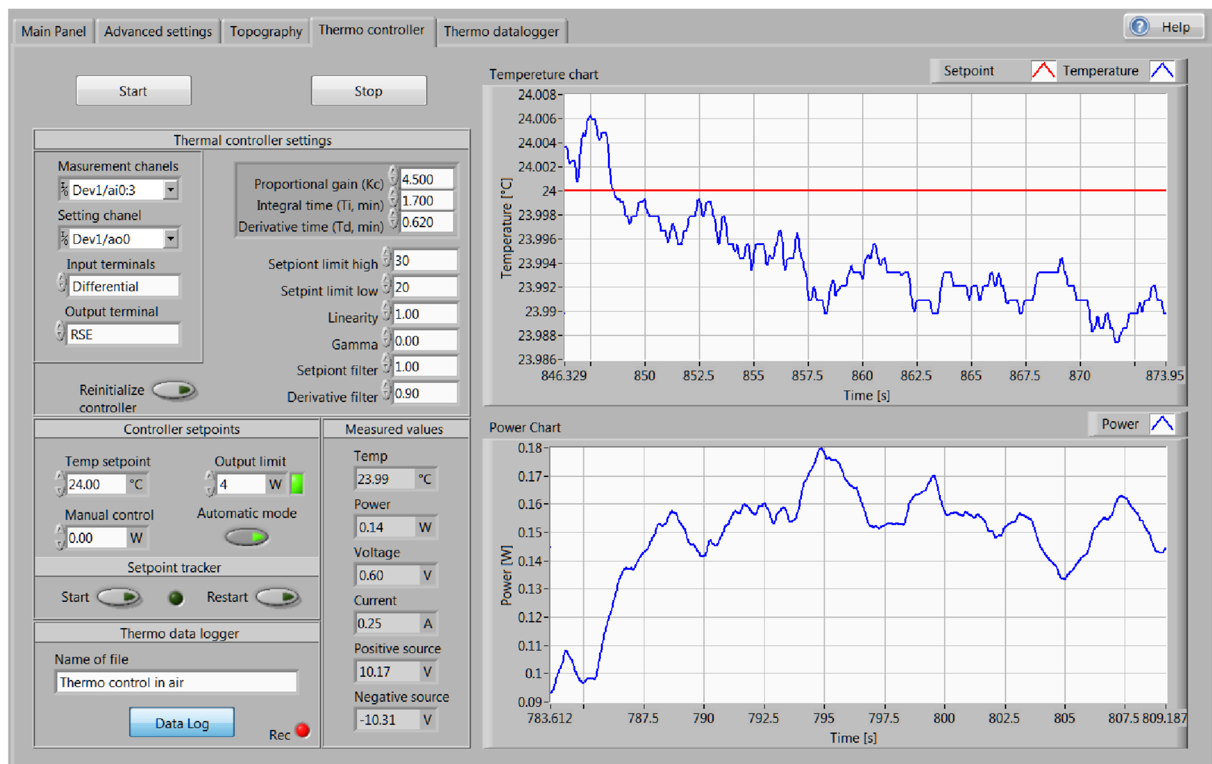

Figure 44: The LabVIEW application - Thermo controller tab

The “Thermo controller” tab contains two charts (see the figure 44); the upper one is the temperature chart which continuously presents the actual measured device temperature and the actual temperature setpoint over last approximately $30\ sec$. The bottom one is the power chart which presents the actual power applied to the Peltier cell also over last approximately $30\ sec$. The carts are updated with every loop of the thermo controller iteration independently on the tab selector therefore in case the other tab is selected the charts are still rolling over and then the thermo controller tab is selected again the charts presents the actual values at the last 30 seconds.

The left upper section is devoted to the NI frontend card setting; first are selected the input (the measurement) channels wherein are the physical channels connected to the hardware. There are selected the first four analog input channels (AI 0:3). Equally the output channel mapping wherein is physically connected the voltage adjustment of the Peltier cell. There is selected first output channel (AO 0).

Then there are selected the NI card terminal configurations; the input channels are connected in the differential mode although it is not required, however the differential mode can suppress the ground loops at the multiple grounded systems. The output channel is connected in the referenced mode and provides the one point grounding between the NI card and the power driver. This NI card setting is saved as the default value for the LabVIEW application and it corresponds with the block diagram presented in the figure 29.

The middle section of the thermo controller tab is devoted to the thermo controller (the PID controller) setting (see the figure 44). The first cluster, which is the most important, contains the PID controller gains whose values was calculated by the Z-N method (see the chapter 6.4.2) due to the system identification by the step response characteristic. However during the thermo controller tests the PID gains was needed slightly adjust to achieve better performance of the thermo control system and especially to suppress the oscillation of the controlled value even at expense of control speed reduction. The gain of the PID controller (K_C) was decreased to value 2.7, the integrative time constant (T_I) of PID controller was increased to value $5.1\ min$ and the derivative time constant (T_D) was slightly increased to vale $1.2\ min$ therefore the derivative part of the PID controller is suppressed by the derivative filter.

The other setting of the PID controller are the “Advanced settings” of the “Advanced PID controller” presented at the block diagram in the figure 29. The first two are the “Setpoint limits” which are not limiting the setpoint at all however the limits are used to calculate the nonlinear integral action and the nonlinear error calculation. This is related to the “Linearity” value setting which is in rage $0 - 1$ and specifies the nonlinear error response wherein the value 1 represents the linear response and the value 0.1 represents an approximately parabolic error response.

The “Gamma” value (see the figure 44) specifies an amount which weighs the control error applied to the derivative part of the controller. The value 0 most avoids the sudden changes in the controller output.

The “Setpoint filter” value do not filters the setpoint value at all however the value specifies the relative emphasis of the setpoint tracking to suppress the disturbances in the controlled variable. The value range is specified to $0 - 1$ and lower value provides the more emphasis to suppress the disturbances in the controlled variable such as the process load changes.

The “Derivative filter” value specifies the derivative filter time constant and increasing this value increases the damping of the derivative action. The value range is defined to $0 - 1$ and the zero value specifies the no derivative filter is applied.

The “Reinitialize controller” button resets the internal PID controller values especially sets the integrative part of controller to zero which avoids its over integrating in case the controller is in the manual control mode. However the controller is automatically reinitialized every time it is switched from the manual to the automatic control mode therefore the LabVIEW controller do not contains the basic bumpless or the anti-windup systems.

In the middle of the thermo controller tab is the “Controller setpoint” section there is set the temperature setpoint, the power limit of the Peltier cell and the power applied to the Peltier cell in case the manual control mode is selected. The square green indicator presents the undervoltage lockout system is properly operating and the power supply voltages are in the specified ranges to correctly provide the system measurements. The automatic mode can be selected by the oval switch and the green indicator presents the automatic mode is running.

Another section is the “Setpoint tracker” (see the figure 44) which is triggered by the “Start” button then the special function named “PID Setpoint Profile” (see the figure 45) starts to reaching the next point of the user defined trajectory. The thermo setpoint trajectory is set in the “Advanced settings” tab in point by point form. The green round indicator announces the thermo trajectory tracker is in progress and then it reaches the last point of defined trajectory the indicator is extinguished. However the trajectory is still preserved in the advanced setting tab and the trajectory can be any time repeated by the “Restart” button.

The bottom section of the thermo controller tab (see the figure 44) is devoted to the thermo data logger which stores the actual device temperature, the actual temperature setpoint, the actual Peltier cell power and the actual time to the binary file with the controller sample period $25\ ms$. The binary files cannot be loaded by any other application therefore it requires the LabVIEW binary file decoder with the defined data structure to decode this files however there is prepared the special tab panel to process and export the thermo data log files to standard text file. The binary file is used therefore the storing to this file type is more straightforward and faster for programs (do not require any conversions) than the other file types.

To log the thermo data file is needed only to fill the file name and click to the “Data log” button then the red round indicator announces the data are logging. The file is located in the application directory and in the “Thermo data” folder. In case the actual log file exists the thermo data logger do not replace the old file by the new one however adds the number in brackets to the file name and retains both of the files which is a straightforward method how to avoid an application error and do not lose any data.

The last middle section of the thermo controller tab (see the figure 44) is presenting the actual status of the thermo controller, specifically: the actual device temperature, the actual power of the Peltier cell, the actual voltage applied to the Peltier cell, the actual current passing the Peltier cell and the actual positive and negative power supply voltages.

7.3.2 The thermo controller application code

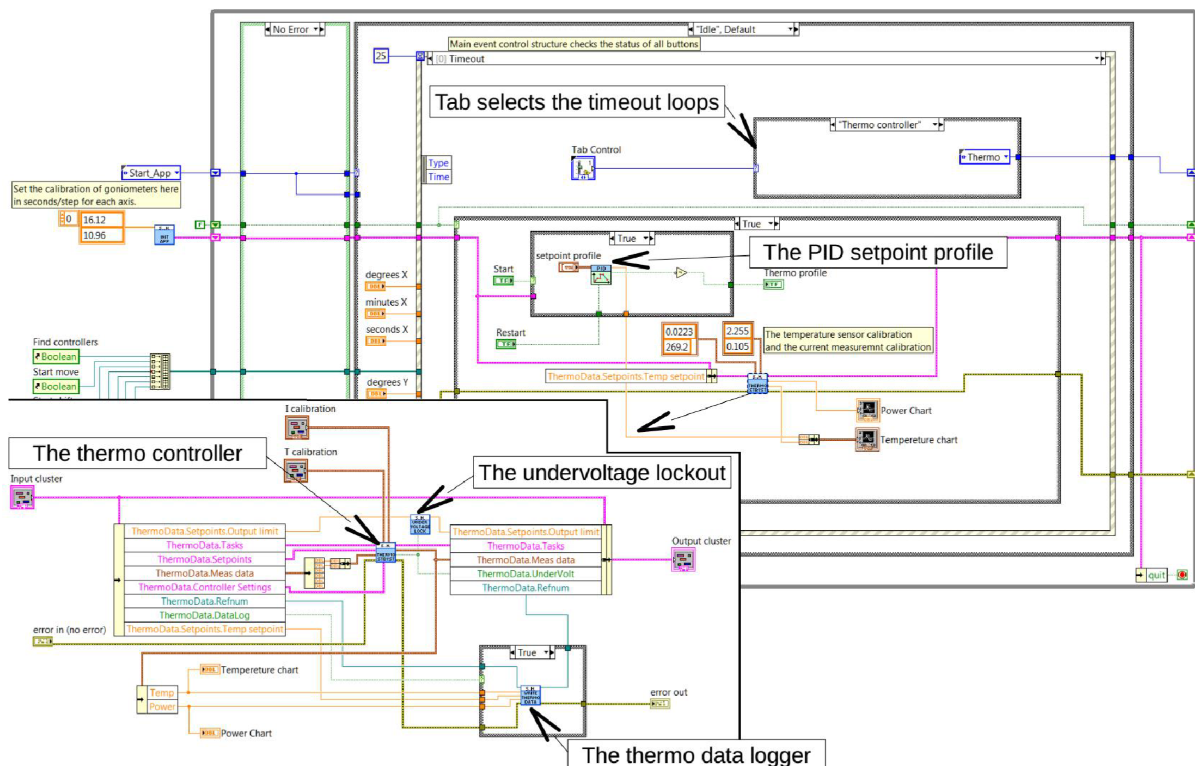

Figure 45: The thermo controller and the timeout loop of the LabVIEW application code

The thermo controller has the structure presented in the chapter 6.4 which is placed to the sub VI named “Thermo controller step by step” and this VI is located in the main event structure timeout loop (see the figure 45). Importantly the thermo controller code is executed independently on the tab selector and therefore if any tab is selected the thermo controller is still refreshing with $25\ ms$ period. However to avoid the application will stop to refresh the timeout loop any popup windows are permitted. For this purpose the application code has the information channel (see the green dot line in the figure 45) which suppresses all of the popup windows in all code cases.

Nevertheless the “Measurement System” application can fully provide almost all of the features except the “Goniometer orientation” setting therefore this feature is controlled only through the popup window.

The figure 45 presents the timeout loop of the main event structure. The small case structure controlled by the tab selector toggles the timeout loop according to the actually selected tab at the application front panel and therefore only the appropriate code is executed. However the thermo controller code must be executed in any tab and therefore the thermo controller code is placed to the main event structure timeout case.

The thermo controller code is activated by the “Start” button which triggers the main event structure and starts to search the appropriate hardware. Then the program makes the appropriate hardware setting and starts the measurement tasks (the input/output task). This is provided by the NI card drivers and the relevant VIs in LabVIEW code. The properly started measurement tasks and saved (the reference) to the main data cluster and then is set the information channel (the green dots in the figure 45) to true and the thermo controller code is activated. However in case the measurement tasks are not properly opened the LabVIEW cannot communicate with appropriate hardware (a wrong setting or the hardware is missing) therefore the application shows an error and the thermo controller is not activated.

The “Stop” button has a similar function as the “Start” button therefore the button triggers another case of the main event structure and it starts to terminate the measurement tasks to properly disconnect the hardware. Then the measurement tasks are properly terminated the information channel is turned to false value and the thermo controller is deactivated. However in case the user triggers the “Stop” button and the measurement tasks do not exist (was ended before or do not start yet) the program skip the termination process and avoids an error. Importantly the “Exit” button at the main panel tab has the same function and the thermo controller is also terminated properly.

The thermo controller is placed to the sub VI visible in the timeout loop (see the figure 45) and the left bottom side of the figure presents the inside structure of the sub VI. This structure also contains the sub VIs and the structure is similarly to the thermo controller block diagram presented in figure 31. There are firstly read out the required data from the main data cluster and then are forwarded to the thermo controller; especially: the measurement tasks, the controller setpoints cluster (contains the temperature setpoint, the power limits and the manual control setpoint), the previous measured data cluster (the temperature and the power) and the controller setting cluster (contains the PID gains and the advanced controller setting presented in chapter 7.3.1).

The thermo controller block (see the figure 45) calculates the controller output (the voltage) which is then forwarded to the hardware and concurrently are the hardware measurements taken. The new measured values (the temperature, the current, the power and the also voltage) are stored to the main data cluster and hereby the values at front panel can be updated by the next code sections in the selectable tabs and certainly are prepared for the next controller calculation. However the temperature and the power charts must be updated in the main timeout loop to achieve their data topicality.

The thermo controller block (see the figure 45) also contains the power supply voltage measurement and in case the voltages are not in the defined ranges ($\pm 9\ V$) the thermo controller block set the output “Undervoltage lockout” to logical true. This signal is then forwarded to the “Undervoltage lockout” block which starts to periodically decrease the power limits of the controller (each period decrease the power limit by $0.1\ W$) until the undervoltage lockout bit is set to false value. However the undervoltage lockout system has its reaction effect one step behind the thermo controller (see the figure 45).

The last block at the thermo control system is the thermo data logger (see the figure 45) which is started by latching the “Data log” button. The button triggers the main event structure case which creates the thermo data log file, save its reference to the main data cluster and activates the thermo data logger code block and then the thermo data logger starts to log the data. In case the “Data log” button is unlatched the event structure is triggered again and another part of code properly close the file. However in case the thermo controller is terminated and the data logger is still running the file is also closed to prevent the file damage.

7.3.3 The thermo data logger tab

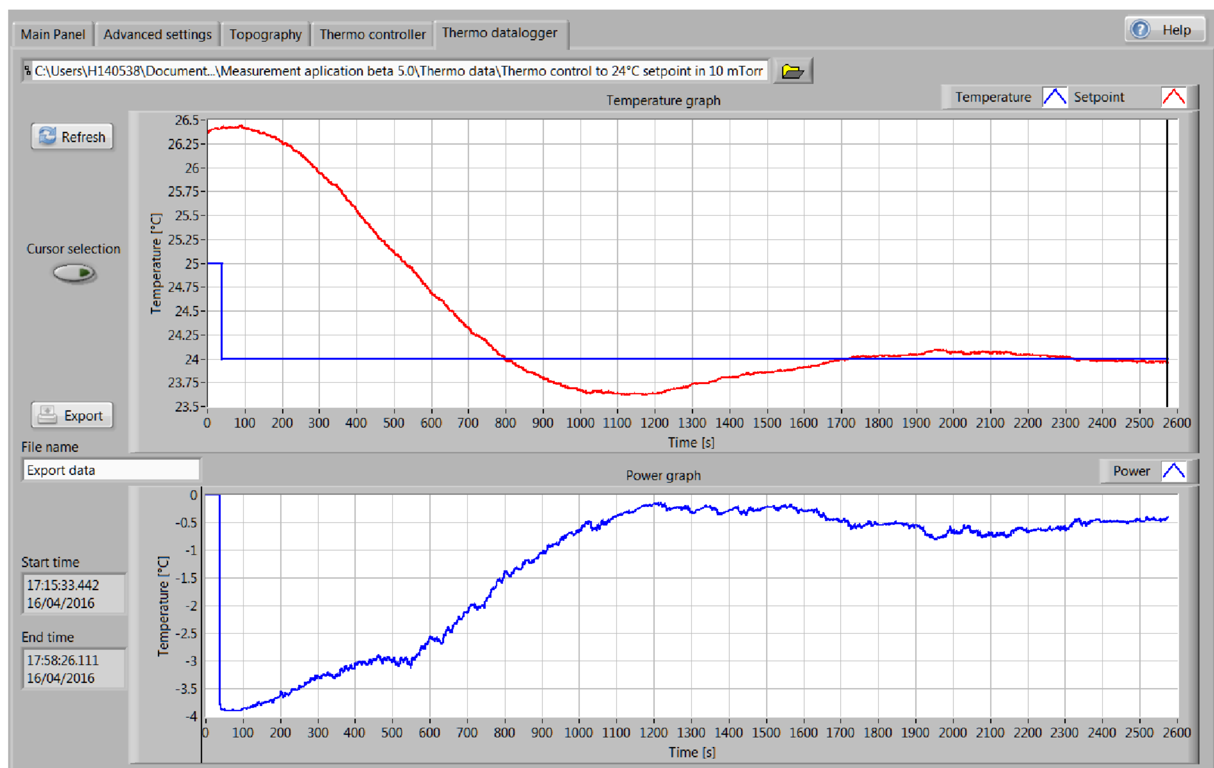

Figure 46: The thermo data logger tab in the Measurement system (the setpoint step in a vacuum)

The thermo data logger tab contains two graphs which are presenting the logged thermo controller data over acquisition time. The first chart presents the temperature and the temperature setpoint and the second graph presents the Peltier cell power in the time dependence. The logged data in the temperature graph can be also focused by the cursors (the black lines) for more closely the temperature curve or the power curve investigation. The acquisition time (the start and the end time) is also presented in the two boxes at left side of the panel in the full form contains the hours, the minutes, the seconds and fractal seconds, the months, the days and the years of the acquisition).

The thermo log file is selected by the path in the upper section of the thermo data logger tab (see the figure 46) or can be also selected by the windows explorer through the folder button. The thermo log files are located in the “Thermo data” folder in the application directory. Default application path is to the LabVIEW folder in the user’s documents folder.

The “Refresh” button in the thermo data logger tab (see the figure 46) triggers the main event structure which once time reads the thermo log file and shows the results in the graphs. In case the “Cursor selection” switch is latched the next iteration of the refresh button will plot only the selected time sequence of the data to the graphs. However the cursor positions can be reset by unlatching the cursor button and refresh the thermo log data again. The thermo log files can be very large especially in the long time acquisition sequences and therefore the thermo data logger cannot be placed to any loop and must be executed only once time which avoids the high hardware requirements of the application.

The last feature of the thermo data logger tab is the function to exports the thermo data log files to the text tabulator delimited data file. The “Export button” triggers the main event structure case which once time reads the binary thermo data log file and save them to the text file with a header. Importantly the file is exported only from the cursor selected part of the graphs which is useful to trim the exported thermo data. Then the text file is exported to the “Thermo exports” folder which is located in directory together with the “Measurement system” application. The exported text file can be imported by many other programs especially the MATLAB. The text file contains the heading columns of the following data: the temperature setpoint, the measured temperature, the measured power, the second counter and the special time stamps (see the figure 47).

	A	B	C	D	E	F
1	Setpt	Temp	Power	Second	Time	Date
2	25	26.37	0	0	3:59:38 PM	3/14/2016
3	25	26.37	0	0.027	3:59:38 PM	3/14/2016
4	25	26.37	0	0.054	3:59:38 PM	3/14/2016
5	25	26.369	0	0.081	3:59:39 PM	3/14/2016
6	25	26.369	0	0.108	3:59:39 PM	3/14/2016

Figure 47: The example of the exported thermo log file imported to the spreadsheet file editor

7.3.4 The thermo control system performance

The thermo control system performance was tested in the vacuum $1.33\ Pa\ (10\ mTorr)$ as well as in an ambient pressure. The controller performance is usually tested as the setpoint step response of the closed controller loop (the controller, the system and the feedback). Then from the step response characteristic can be read out the fundamental information representing the thermo control system performance.

The setpoint step response presented in the figure 46 was measured in the vacuum chamber, the controlled system was presented in the figure 29 and the controller settings was presented in the figure 44. The setpoint step starts at the time $330\ sec$ from the ambient temperature approximately $26.3\ °C$ to the temperature setpoint $24\ °C$ (see the figure 46). The controller reaches the setpoint (the 90 % of the full step) after approximately $700\ sec$ and there are two visible overshoots of the controlled variable; the two visible overshoots are usually considered as the optimal controller setting. The first overshoot has amplitude approximately $0.35\ °C\ (15\ \%\ of\ the\ full\ step)$ and the second overshoot has amplitude approximately $0.1\ °C\ (4\ \%\ of\ the\ full\ step)$. The overshoot under $20\ \%$ in the amplitude of the full step is usually also considered as the good controller performance.

However the Zero Rate Output measurements can start after the full temperature stabilization which the controller is achieved at the time approximately $50\ min$. The long time sequence needed to stabilize the temperature is mostly caused by the time response of thermal conductors (heat pipes) and also by the high thermal capacitance at the copper plates. For the comparison of the controller performance at the vacuum and at an ambient pressure conditions, there was also measured the temperature setpoint step response of the thermo control system in an ambient air pressure (see the figure 48).

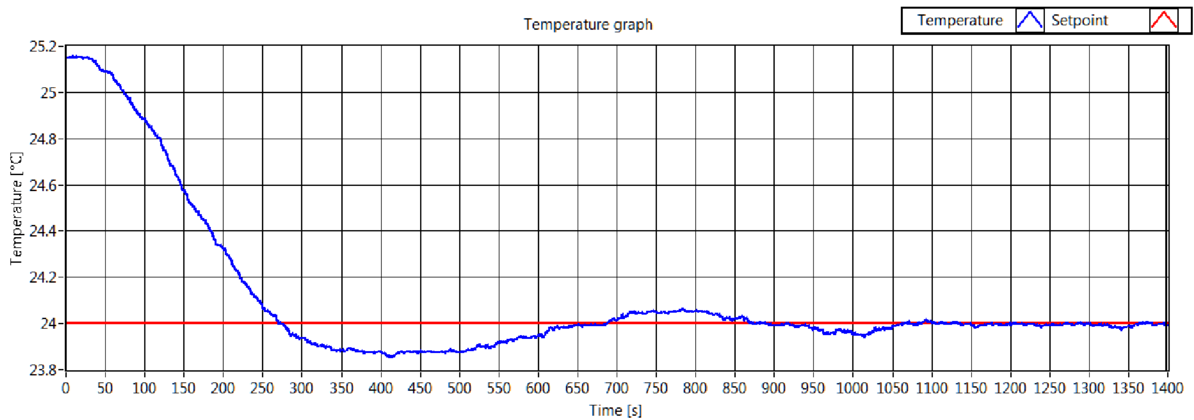

Figure 48: The temperature setpoint step response in an ambient pressure

The setpoint step starts at the approximately $0\ sec$ point of the graph in figure 48 and from the ambient temperature approximately $25.2\ °C$ to the temperature setpoint $24\ °C$. The controller reaches the setpoint (the $90\ \%$ of the full step) after approximately at $250\ sec$ and there are three visible overshoots of the controlled variable. The first overshoot has amplitude approximately $0.15\ °C\ (13\ \%\ of\ the\ full\ step)$, the second overshoot has amplitude approximately $0.06\ °C\ (5\ \%\ of\ the\ full\ step)$ and the third is approximately $4\ \%$. The full temperature stabilization is achieved after approximately $20\ min$.

However the step response in air is measured only from the temperature $25\ °C$ instead of $26\ °C$ therefore the controller performance can be faster due to lower temperature setpoint step. Anyway the thermo control system performance is approximately two times faster in an ambient pressure than the performance in the vacuum.

The last tested feature of the thermo control system is the ability of the controller to track the user defined trajectory. However due to the controlled system has high dynamic the temperature setpoint trajectory is the linear function (the ramp) with low slope. The presented temperature setpoint ramp (see the figure 49) has slope $0.04\ °C/min$ and starts from the stabilized temperature setpoint $24\ °C$ from the last test (see the figure 46) and ends in temperature $26\ °C$ at the time $50\ min$.

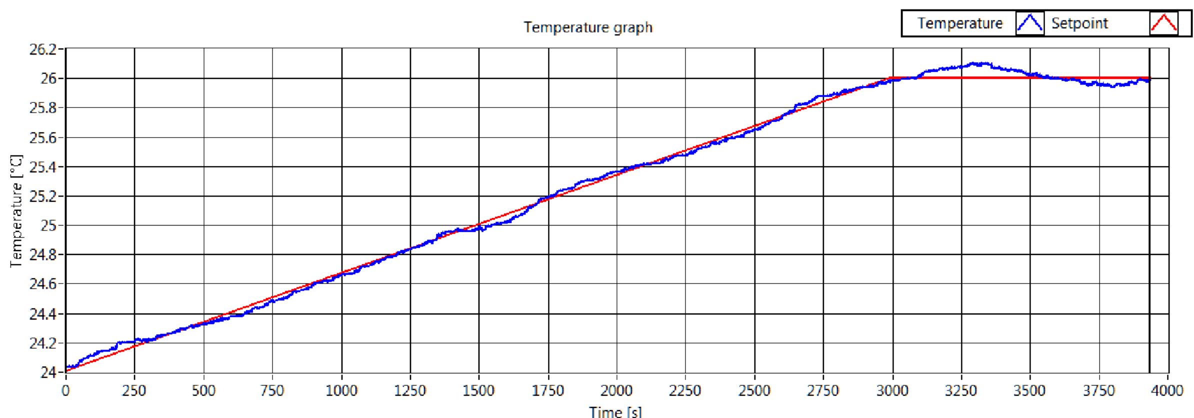

Figure 49: The temperature setpoint ramp in the 1.33 Pa vacuum

The controller is able to track the defined trajectory with maximal deviation $0.08\ °C$ at the temperature approximately $25\ °C$ and then the overshoot at the end of the ramp is $0.1\ °C$. The Peltier cell power needed to achieve this trajectory is only approximately $0.5\ W$ therefore the controller is capable to achieve the setpoint trajectory with higher slope however the controller must use more of the power reserves in the system dynamics and due to the thermo control system can start to slightly oscillate along the trajectory (see the figure 50 and 51).

The temperature setpoint trajectory was also tested in an ambient pressure and moreover there is used more complex trajectory consisting of the two ramps with different slopes. The first descending ramp is similar to the ramp used for the controller test in the vacuum and its slope is $0.03\ °C/min$ followed by short pause to stabilize the temperature and then the second ascending ramp with slope $0.12\ °C/min$.

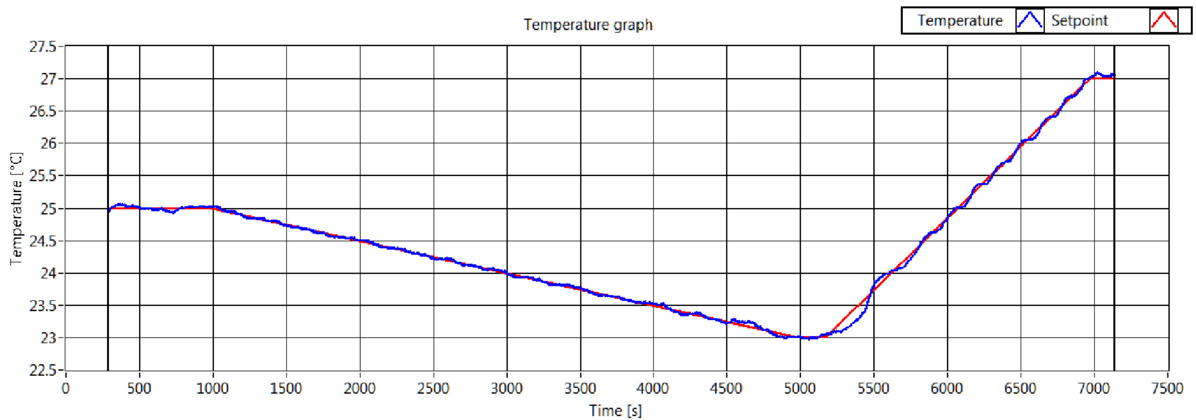

Figure 50: The temperature trajectory in an ambient pressure

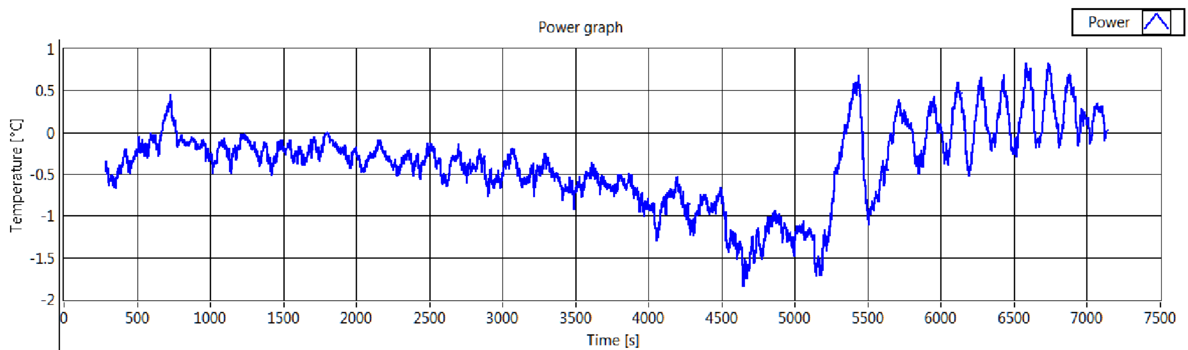

Figure 51: The appropriate Peltier cell power to the temperature trajectory

The thermo control system is able to fairly accurately track the first defined trajectory with lower slope. The maximal deviation of this descending temperature setpoint trajectory is approximately $0.1\ °C$ (see the figure 50) and the power curve is relatively smooth (see the figure 51). On the other hand the second temperature setpoint trajectory with a much higher slope is on the limit of the controller and the Peltier cell power starts to slightly oscillate and also the device temperature is slightly oscillating around the temperature setpoint trajectory.

However the thermo control system in an ambient pressure is able to control the system temperature over this high slope trajectory with relatively good performance and the maximal deviation of the temperature is approximately $0.25\ °C$. The controller ability to track the trajectory slope in the vacuum is approximately twice worse than in an ambient pressure and therefore the thermo control system in the vacuum starts to oscillate around the trajectory with slope approximately $0.06\ °C/min$.

All of the presented graphs and others are available in the thermo data log files included in document annex and can be any time loaded by the thermo data logger tab in the "Measurement System". The data are also exported to the tabulator delimited text files.

8 THE GYROSCOPE NOISE ANALYSIS

The gyroscope performance is highly dependent on the quality of the vacuum surrounding the gyroscope structure. The surrounding pressure of the medium (typically the air) is influencing the MEMS gyroscope performance by the two fundamental ways; the ambient pressure must be as low as possible to achieve the high Q-factor of the gyroscope resonator due to lower damping of the proof mass movement.

8.1 THE GYROSCOPE NOISE OVER QUALITY OF THE VACUUM

Factually the non-ideal vacuum conditions causes the higher damping of the proof mass movement. Therefore the noise over the quality of the vacuum for the MEMS rate element was investigated to find the function between the noise and the vacuum level.

Certainly the gyroscope structure must by placed to the vacuum pressure to achieve the stable drive vibrations of the proof mass at the resonance frequency. The point of the interest is focused to the pressure levels of the deep vacuum and their influence to the gyroscope performance. The investigated pressure levels are around $13.33\ Pa\ (100\ mTorr)$ which are usually considered as the very low pressure levels.

The unpackaged MEMS gyroscope sample is placed to the vacuum chamber (see the figure 26 or 29) then the air is exhausted to the specific pressure value and then is measured the long term data acquisition (over 10 hours) of the tested gyroscope output in stable position and the gyroscope bias value is estimated. The vacuum pressure level is measured by the Active Pirani/Cold Cathode Vacuum gauge (see the figure 52). The vacuum pressure level is then controlled by the LabVIEW controlled vacuum pump.

The parameters of the vacuum gauge:

- Range: $13332\ Pa\ - 0.66\ \mu Pa$
- Accuracy: $\pm 30\ \%$
- Repeatability: $\pm 5\ \%$

Figure 52: The vacuum gauge [19]

The RMS value of the MEMS rate element long term data output (the RMS noise) allowing comparison of the different MEMS rate elements performance at various vacuum levels was chosen.

The first data set was acquired for $13.33\ Pa\ (100\ mTorr)$ vacuum level and the measurement duration was approximately $12\ hours$. The MEMS gyroscope was integrated to the Honeywell proprietary front end electronic design in the stable position (no input rate). The output signal is acquired by the LabVIEW application with sample rate of$100\ Hz$.

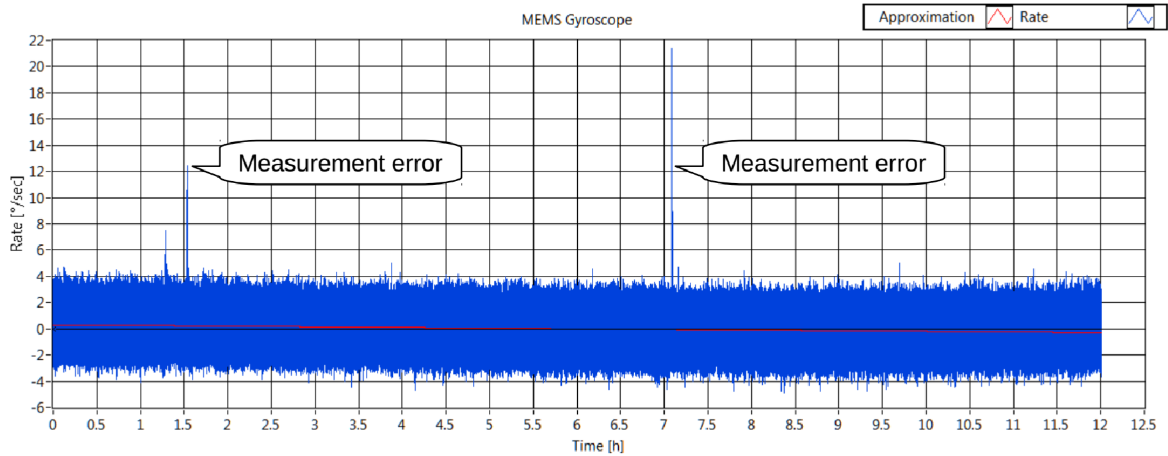

Figure 53: MEMS gyroscope output noise in stable position and 13.33 Pa vacuum.

The RMS noise value is estimated as the RMS value of all the measured gyroscope output samples. The figure 53 presents the samples of the gyroscope rate over $12\ hours$ in the $13.33\ Pa\ (100\ mTorr)$ vacuum and the acquisition set contains over $4\ million$ samples. In some cases there occurs the unpredictable measurement errors (see the figure 53) which can be caused by disturbances in the electronic setup or by the acquisition software. These measurement errors do not represent the MEMS gyroscope performance and moreover are highly suppressed by the RMS estimation however for better performance responsibility are these measurement errors eliminated from the measurement data set.

The measured noise (the data set) of the gyroscope output used for the estimation of the RMS noise value is presented in the figure 54. The measured MEMS gyroscope output noise has the maximal amplitude approximately $\pm 4.5°/sec$ of the gyroscope angular rate output and very low descending trend with the slope $-0.05°/\sec\ per\ hour$.

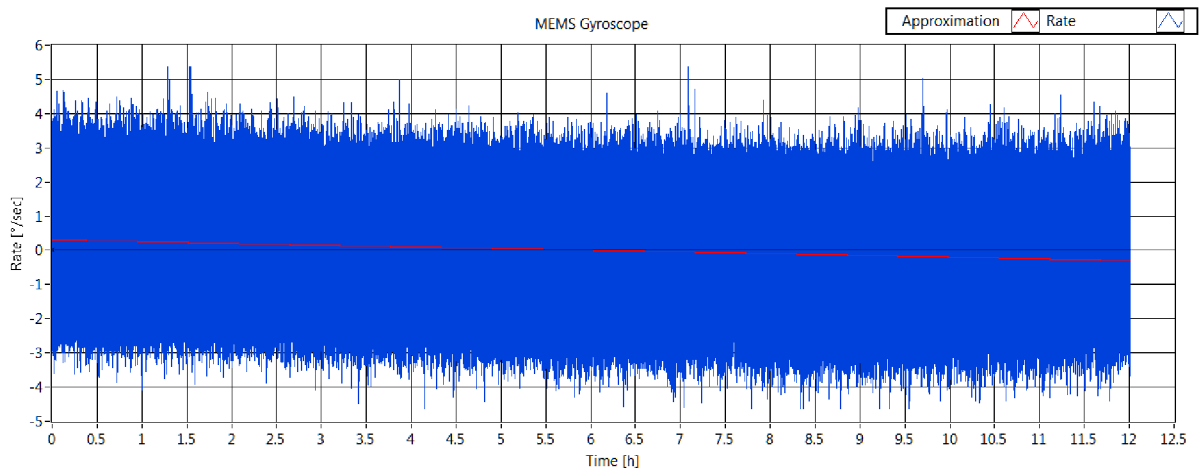

Figure 54: The coerced MEMS gyroscope output noise in stable position and 13.33 Pa vacuum

After the first measurement in $13.33\ Pa$ pressure was the vacuum level decreased to the value $6.66\ Pa\ (50\ mTorr)$ and another $12\ hours$ data set of the MEMS gyroscope angular rate output was measured. The last value of RMS noise is then measured in $1.33\ Pa\ (10\ mTorr)$ vacuum level. The data set is then coerced and the measurement errors are also eliminated. All of the data sets has trimmed the mean bias level to the zero value (see the figure 54). The RMS value of the measured noise is then calculated as the RMS value of all samples with trimmed bias level for the individual data sets. The appropriate values are then introduced into the table 2.

Table 2: The MEMS gyroscope output RMS noise value over vacuum level

Vacuum level	13.33 Pa 100 mTorr	6.66 Pa 50 mTorr	1.33 Pa 10 mTorr
RMS noise	$0.97\,°/sec$	$1.14\,°/sec$	$1.38\,°/sec$

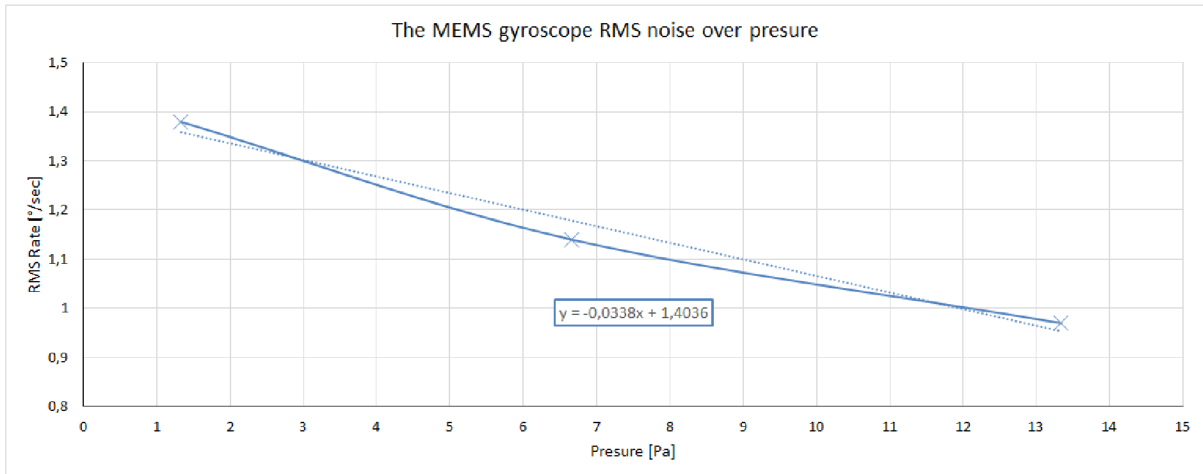

Graph 1: The MEMS gyroscope output RMS noise value over vacuum levels

The table 2 and the graph 1 represents the function of the gyroscope RMS noise over the vacuum quality level. There is visible the descending trend with approximately linear trend of the gyroscope RMS noise on the medium pressure surrounding the gyroscope structure. The RMS noise is decreased by approximately $2.5\ \%$ with any $Pascal$ of vacuum pressure. The dependence is measured in one decade of the vacuum pressure level.

The MEMS gyroscope output angular rate has lower RMS noise in the higher pressure levels. This dependence certainly cannot continue to the higher pressure levels over $13.33\ Pa$ therefore the high vacuum pressure highly decreases the Q-factor of the MEMS resonator. The vacuum levels over $100\ mTorr$ cannot be measured as it is out of the range of the vacuum pump due to the magnetic bearing of the vacuum pump molecular turbine.

The main objective of this activity was to test the measurement set-up for the long term data acquisitions in the different vacuum levels. The design was properly working for more than a week in the deep vacuum and the first noise analysis of the MEMS gyroscope was acquired. The temperature of the electronic design was approximately 50 °C for all measurements. The higher temperature is needed to achieve a good long term cooling capabilities of all devices in the vacuum chamber.

9 CONCLUSION

The conclusion is divided to two parts. The first parts presents the summary of the diploma thesis and its compliance with the assigned objectives. The second part presents the achieved performance of the developed “Measurement System” application for the MEMS gyroscope testing as well as the discussion the tests of the MEMS gyroscope sample.

9.1 THE SUMMARY

The theoretical part of this thesis introduces the key parameters of the angular rate sensors manufactured by the MEMS technology (MEMS gyroscopes). The working principle of the classical gyroscope and then the MEMS gyroscope is described. The key parameters of the MEMS gyroscopes (Q-factor, Bias, Scale factor, etc.) are discussed in the chapter 2. Subsequent chapter is devoted to short introduction to MEMS gyroscope designs and the principles of operation are described (single mass, double mass, vibrating ring, decoupled gyroscopes, etc.).

The practical part of thesis contains the introduction to the individual measurement chain parts (Polytec MSA-500 system, the goniometer stages and the thermal control system) which are used to MEMS gyroscope testing. The practical part is then mostly devoted to the description of the LabVIEW application: “Measurement System” developed as a result of the preparation of the thesis. The application is capable to fully control the two goniometer stages and align the tested device surface to the perpendicular orientation with respect to the Polytec MSA-500 measurement head using the topography measurement. The application also provides feature to control and stabilize the temperature of the tested device using the Peltier cell and the heat conductors according to the diploma thesis assignment.

The Polytec MSA-500 is complex system which combines three individual systems i.e. Scanning Laser-Doppler Vibrometer for out-of-plane measurement, the Stroboscopic Video Microscopy for in-plane measurement and the Topography Measurement System for surface metrology. The chapter 4 is devoted to short introduction of these three systems. The description of the goniometer stage and the specification of the Standa goniometer stages and the Standa goniometer controller used for the angular compensation of the tested surface is presented in the chapter 5.

The chapter 6 is dedicated to the thermo-electric cooler specification using the Peltier cell. The Peltier cell controller which uses the LabVIEW software to control the tested device temperature developed within the thesis is described as well. The NI USB-6001 acquisition card is used as a front end and together with the power driver it controls the power of the Peltier cell. Concurrently the NI card measures the system variables as the Peltier cell current and the device temperature. The electrical wiring of the power driver and the block diagram of the thermo control system is also described in the chapter 6.

Moreover in the chapter 6 the structure of the software thermo controller which contains the cascade connection of two controllers is described. The power PI controller controlling the power of the Peltier cell and the temperature PID controller controls the temperature of the tested device. Lastly the process of setting the PID controller constants using the system power step response and the Ziegler Nichols method is described.

The developed LabVIEW application named the “Measurement System” is entirely described in the chapter 7. The application requires the connection of the goniometer controller and the Peltier cell driver to be fully operational. However, the application is also executable in any LabVIEW environment independently on the hardware connection and only the parts which controls the goniometer stages and thermo control system are unavailable. The application can load and present the topography maps and also present the temperature and the Peltier cell power charts for the later data analysis.

The “Measurement System” application is fully executable in the standard National Instruments **LabVIEW 2013 32-bit** environment however the additional **PID and Fuzzy Logic toolkit** [14] and the **NI myDAQ drivers** [15] are required for the properly application start. The application can be started due to “Measurement System” VI located in the **“Measurement System” LabVIEW project**. In the document annex is located the compiled version of the application which is executable in the windows system only however the **LabVIEW run-time engine 2013 (32bit)** [20] and the **NI myDAQ drivers** [15] is needed to be installed. The application also contains the interactive help function which basically explains the operation of the selected application element. The help function is activated by the Help button.

9.2 The performance

The “Measurement System” application is programmed as the state machine algorithm which is controlled by the event structure mechanism as the code cases selector. The application utilizes the idle timeout loop mechanism to its hardware requirements reduction and the appropriate code sections are activated only if it is required by the user activity. The application also allows the periodical code execution using the timeout case of the event structure moreover the timeout section are selected by the tab selector at the front panel of the application. Due to this mechanism the application can combine several systems in the one “Measurement System” and only the required code part is executed. This execution mechanism is described in the flow chart (see the figure 34 at the beginning of the chapter 7).

The first part of the “Measurement System” description is devoted to the goniometer stage controller and its user interface, see the chapter 7.1. The application controls the goniometers through the angular coordinates in the degrees, minutes or seconds which are set in the main panel. Concurrently status information from the hardware controller is also presented in the main panel. There is, inter alia, presented the actual position of each goniometer in degrees, the actual speed of the goniometer in degrees per second as well as the controller power status information.

The accuracy of the goniometer angular adjustment is strictly defined by the goniometer resolution which is defined by the steeper motor revolution per step resolution. The goniometer has basic resolution approximately $10'' - 16''$ depending on the goniometer type. However the goniometer controller also supports the microstepping technique wherein each step is divided to 256 microsteps and the theoretical resolution of the goniometer angular adjustment is lower than $0.07''$.

The main panel of the application also contains the “Cyclic function” for cyclic movement of the goniometers. Each goniometer stage is then cyclically moving with the defined speed, acceleration and deceleration. The range of the cyclic movement is also defined as the maximal positive and negative angle of each goniometer set in the main panel and certainly is limited by the maximal goniometer range which is approximately $\pm 2.5°$. This feature can be also used as the defined angular input for the MEMS gyroscope testing.

The “Advanced settings” panel of the application contains the function which finds the center of the goniometer trajectory and concurrently the maximal goniometer ranges are acquired. This function is useful in cases the goniometer stepper motor lose its step especially in overloaded conditions (exceeding the weight or acceleration limit). The other part of the advanced setting panel contains the goniometer speed, acceleration and deceleration setting. The maximal acceleration/deceleration of the goniometer is approximately $30°/sec^2$ and maximal achievable speed is approximately $15°/sec$.

The “Topography” panel (see the chapter 7.2) is devoted to the angular compensation process which aligns the tested surface of the MEMS element attached to the goniometer stages to perpendicular orientation with respect to the Polytec measurement head due to the Polytec topography measurement system. The accuracy of the alignment system is highly dependent on the topography measurement resolution and accuracy. However the topography accuracy is slightly decreased due to the corrugation effect in the topography map in the Y axis (see the figure 42). The corrugation phenomenon is caused by the mechanical stand oscillations of the Polytec measurement head. Therefore the mechanical attachment of the head has less stiffness in the Y axis. Moreover the waves in the topography map have approximately $300\ nm$ in the amplitude which is complicated to suppress.

The accuracy of the angular alignment system using the topography measurement is approximately $0.0002°$ in the X axis which is considered as a good alignment accuracy and the maximum achievable due to the topography measurement accuracy. The accuracy in the Y axis is much worse due to corrugation phenomenon, however the achieved accuracy is approximately $0.018°$ which is sufficient to minimize the out-of-plane mode misalignment measurement error of the oscillating gyroscope proof masses. The accuracies are obtained as the deviation of the repeated topography measurements and alignment processes. This part of the diploma thesis (the angular compensation system) was also presented at the student competition named EEICT organized by the Brno University of Technology faculty of Electrical Engineering and faculty of Information Technology.

The “Thermo controller” panel (see the chapter 7.3) is devoted to the temperature control system using the Peltier cell. The system is capable to stabilize the temperature of the tested device which is used to the long term data acquisition of the MEMS gyroscope output to Alan variance calculation and evaluation of the key MEMS gyroscope parameters (ARW, bias instability and RRW) without the temperature influences to the gyroscope element or the gyroscope electronics. The absolute accuracy of the temperature stabilization is approximately $\pm 1\ °C$ and the maximal temperature deviation to the temperature setpoint is lower than $1\ \%$. However the time to achieve the stable device temperature is approximately $50\ min$ in the vacuum and approximately $20\ min$ in the ambient pressure.

The thermo control system is capable to achieve any user defined temperature setpoint required for testing the thermal sensitivity of the MEMS element. However the minimal achievable temperature of the tested device is approximately $10\ °C$ and the maximal achievable temperature is approximately $90\ °C$. The temperature range is dependent on the Peltier cell cooling capability and the maximal achievable Peltier cell power which has hardware limited current to $3\ A$ by the Peltier cell driver. The system is also capable to track the user defined temperature trajectory however due to the system dynamic is the maximal achievable temperature slope approximately $0.06\ °C/min$ in the vacuum and approximately $0.12\ °C/min$ in an ambient pressure. The temperature deviation of the setpoint tracking is dependent on the temperature slope and the maximal value is $0.25\ °C$ at the maximal temperature slope. The temperature trajectory can be set in the “Advanced settings” panel as the point by point trajectory.

The thermo control system is capable to log the actual temperature, the actual temperature setpoint, the actual Peltier cell power and the actual time with the controller sample period. The data are logged to the binary file however the data can be anytime loaded in the “Thermo datalogger” panel of the “Measurement system” and there can be presented to better investigation of the temperatures and power curves. The data logger panel is also capable to export the thermo data to tabulator delimited text file with the header which can be then imported to another application (MATLAB, spreadsheet editor, etc.).

The last chapter presents the tests of the new Honeywell International s.r.o. electronic design in the deep vacuum conditions for the MEMS gyroscope noise analysis over the vacuum quality level measurement. There is presented the RMS noise value of the MEMS gyroscope long term output data set. The gyroscope RMS noise is decreasing with the higher vacuum pressure levels by approximately $2.5\ \%/Pa$. The best gyroscope performance is achieved in approximately $13.33\ Pa\ (100\ mTorr)$ vacuum level with RMS noise value $0.97\ °/sec$.

REFERENCES

[1] MEMS & Nanotechnology Exchange: About MEMS. *What is MEMS Technology?* [online]. [last accessed 2015-11-08]. Available from: https://www.mems-exchange.org/MEMS/what-is.html

[2] Wikipedia. *Gyroscope* [online]. [last accessed 2015-11-08]. Available from: https://en.wikipedia.org/wiki/Gyroscope

[3] ZHANG, Zengping, Fuxue ZHANG and Wei ZHANG. Measurement of Phase Difference for Micromachined Gyros Driven by Rotating Aircraft. *Sensors* [online]. 2013, **13**(8): 11051-11068 [last accessed 2015-11-08]. DOI: 10.3390/s130811051. ISSN 1424-8220. Available from: http://www.mdpi.com/1424-8220/13/8/11051/

[4] KEMPE, Volker. *Inertial MEMS: Principles and Practice*. New York, USA: Cambridge University Press, 2011. ISBN 978-0-521-76658-6.

[5] ANCAR, Cenk and Andrei SHKEL. *MEMS Vibratory Gyroscopes: Structural Approaches to Improve Robustness*. New York, USA: Springer Science+Business Media, 2009. ISBN 978-0-387-09535-6.

[6] STOCKWELL, Walter. Bias Stability Measurement. *Crossbow Technology, Inc* [online]. [last accessed 2015-11-20]. Available from: http://www.moog-crossbow.com/Literature/Application_Notes_Papers/Gyro_Bias_Stability_Measurement_using_Allan_Variance.pdf

[7] HE, Guohong a Khalil NAJAFI. A single-crystal silicon vibrating ring gyroscope. *Center For Wireless Integrated MicroSystems University of Michigan, Ann Arbor, Michigan 48109 USA*. 2002.

[8] POLYTEC GMBH WALDBRONN. *MSA-500 Micro System Analyzer*. Waldbronn, 2014. Available from: http://www.polytec.com/it/products/vibration-sensors/microscope-based-systems/msa-500-micro-system-analyzer/

[9] Basic Principles of Vibrometry. *Polytec GmbH Waldbronn* [online]. [last accessed 2015-11-08]. Available from: http://www.polytec.com/us/solutions/vibration-measurement/basic-principles-of-vibrometry/

[10] 8MG99 - Motorized Goniometer. *Standa: Opto-Mechanical Products* [online]. ©2000-2015 [last accessed 2015-11-08]. Available from: http://www.standa.lt/products/catalog/motorised_positioners?item=72

[11] OSTEN, Wolfgang. *Optical inspection of microsystems*. Boca Raton, FL: CRC/Taylor, c2007, p. 245-269. Optical science and engineering (Boca Raton, Fla.), 109. ISBN 9780849336829.

[12] The Peltier Effect and Thermoelectric Cooling. PHYSICS 212 WEB PROJECT. *The Physics of Cooling Techniques* [online]. 2007 [last accessed 2015-11-08]. Available from: http://ffden-2.phys.uaf.edu/212_spring2007.web.dir/sedona_price/phys_212_webproj_peltier.html

[13] Syntéza. *Katedra automatizační techniky a řízení Fakulta strojní VŠB - Technická univerzita Ostrava* [online]. [last accessed 2015-12-28]. Available from: http://www.352.vsb.cz/uc_texty/Identifikace/synteza/synteza.htm#start

[14] LabVIEW 2013 PID and Fuzzy Logic Toolkit [online]. *www.ni.com:* National Instruments Support, 2013 [last accessed 2016-04-13]. Available from: http://www.ni.com/download/labview-pid-and-fuzzy-logic-toolkit-2013/4212/en/

[15] NI myDAQ Driver [online]. *www.ni.com:* National Instruments Support, 2012 [last accessed 2016-04-13]. Available from: http://www.ni.com/product-documentation/12403/en/#toc1

[16] ALPER, Said Emre. *MEMS gyroscopes for tactical-grade inertial measurement applications.* 2005. PhD Thesis. MIDDLE EAST TECHNICAL UNIVERSITY. Available from: https://etd.lib.metu.edu.tr/upload/12606483/index.pdf

[17] CHIDAMBARAM, Vivek, Xie LING and Chen BANGTAO. Titanium-Based Getter Solution for Wafer-Level MEMS Vacuum Packaging. *Journal of Electronic Materials* [online]. 2013, **42**(3), 485-491 [last accessed 2016-04-23]. DOI: 10.1007/s11664-012-2350-9. ISSN 0361-5235. Available from: http://link.springer.com/10.1007/s11664-012-2350-9

[18] SPARKS, Douglas, Jay MITCHELL and Sangwoo LEE. Output Drifting of Vacuum Packaged MEMS Sensors Due to Room Temperature Helium Exposure. *Journal of Sensor Technology* [online]. Scientific Research, 2013, 2, 101-109 [last accessed 2016-04-23]. Available from: http://file.scirp.org/pdf/JST_2013122009560886.pdf

[19] Pfeiffer Compact FullRange Gauge PKR 251. *Ideal Vacuum Products* [online]. Albuquerque, New Mexico: Ideal Vacuum Products, LLC, 2014 [last accessed 2016-04-24]. Available from: http://www.pchemlabs.com/product.asp?pid=3214

[20] LabVIEW Run-Time Engine 2013 [online]. *www.ni.com*: National Instruments support, 2013 [last accessed 2016-05-13]. Available from: http://www.ni.com/download/labview-run-time-engine-2013/4059/en/

LIST OF ATTACHMENTS

- The electronic version of the diploma thesis.
- The datasheets:
    - Goniometer controller - Programming manual.pdf
    - Goniometer controller - User manual.pdf
    - Goniometer controller library for Labview_2.8.4
    - NI-USB-6001 acquisition card.pdf
    - Operational amplifier LM358.pdf
    - Peltier cell – 51.8W.pdf
    - PID and Fuzzy control toolkit user manual.pdf
    - Power amplifier OPA548T.pdf
    - Temperature sensor AD590.pdf
    - Thermal compound - graphite pad.pdf
- The compiled LabVIEW application:
    - The “Measurement system.exe”
    - The additional contends in “subVI” folder.
    - The driver functions for goniometer controller in “libximc.dll” file in data folder.
    - The measured thermo log files in “Thermo data” folder.
- The measured performance of the thermo control system in ASCI files contains the “Thermo exports” folder.
- The measured topography maps in ASCI files contains the “TMS measurement” folder.